An Automated Modified Region Growing Technique for Prostate Segmentation in Trans-Rectal Ultrasound Images

by

Marian Wahba

A thesis

presented to the University of Waterloo

in fulfillment of the

thesis requirement for the degree of

Master of Applied Science

in

Electrical and Computer Engineering

Waterloo, Ontario, Canada, 2008

I hereby declare that I am the sole author of this thesis. This is a true copy of the thesis, including any required final revisions, as accepted by my examiners.

I understand that my thesis may be made electronically available to the public.

Abstract

Medical imaging plays a vital role in the medical field because it is widely used in diseases diagnosis and treatment of patients. There are different modalities of medical imaging such as ultrasounds, x-rays, Computed Tomography (CT), Magnetic Resonance (MR), and Positron Emission Tomography (PET). Most of these modalities usually suffer from noise and other sampling artifacts. The diagnosis process in these modalities depends mainly on the interpretation of the radiologists. Consequently, the diagnosis is subjective as it is based on the radiologist experience.

Medical image segmentation is an important process in the field of image processing. It has a significant role in many applications such as diagnosis, therapy planning, and advanced surgeries. There are many segmentation techniques to be applied on medical images. However, most of these techniques are still depending on the experts, especially for initializing the segmentation process. The artifacts of images can affect the segmentation output.

In this thesis, we propose a new approach for automatic prostate segmentation of Trans-Rectal UltraSound (TRUS) images by dealing with the speckle not as noise but as informative signals. The new approach is an automation of the conventional region growing technique. The proposed approach overcomes the requirement of manually selecting a seed point for

initializing the segmentation process. In addition, the proposed approach depends on unique features such as the intensity and the spatial Euclidean distance to overcome the effect of the speckle noise of the images. The experimental results of the proposed approach show that it is fast and accurate. Moreover, it performs well on the ultrasound images, which has the common problem of the speckle noise.

Acknowledgements

I would like to thank my research group, Medical Image Analysis and Machine Intelligence (MIAMI) group, at the University of Waterloo. Special Thanks to my supervising professor, Prof. Magdy Salama for his support, guidance, fruitful discussions, and encouragement throughout my entire graduate studies and the writing of this thesis.

Words fall short of expressing my love, appreciation, and gratitude for my caring husband, Albert, for his love, understanding, and support throughout the course of this work. He was always there for me. And my beloved kids Andrew, and Veronika whose innocent faces made it easier.

Contents

List of Figures

List of Tables

Chapter 1

INTRODUCTION

Medical images are the key assets which provide means for health care professionals to evaluate patients for diagnosis and treatment. Hence, the vision that drives the medical imaging analysis and processing is an important factor in improving the patient health. Studying medical images depends mainly on the visual interpretation of the radiologists. However, this consumes time, besides, it is usually subjective as it varies according to the experience of the radiologists. Due to the aforesaid considerations, using computer-aided image analysis techniques becomes a necessity, in order to facilitate analyzing and processing different medical image modalities. All image techniques can be grouped under a general framework-Image Engineering (IE), which consists of three layers: image processing (low layer), image analysis (middle layer), and image understanding (high layer), as shown in Fig. 1.1. In recent years, image engineering has formed a new discipline and made great

progress. Image segmentation is the first step and also one of the most critical tasks of image analysis, which has the objective of extracting information (represented by data) from an image via image segmentation, object representation, and feature measurement as shown in Fig. 1.1. It is evident that the results of segmentation will have considerable influence over the accuracy of feature measurement [1].

Computerized medical image segmentation plays an important rule in medical imaging applications. It is widely used in different applications such as diagnosis, localization of pathology, study of anatomical structure, treatment planning, and computer-integrated surgery. However, medical image segmentation remains a hard problem due to the variability and the complexity of the anatomical structures in the human body. Besides, there is a wide variety of medical imaging modalities. Most of these modalities suffer from the presence of noise and sampling artifacts. These problems can significantly affect the results of the segmentation. There are different techniques used for medical image segmentation, each of which has its advantages, and disadvantages, as it will be discussed in chapter 3. In the sense of computerized segmentation techniques, it should be expected that these techniques are automatically performed. However, it is not exactly the case because most of them still need at least some sort of manual interaction.

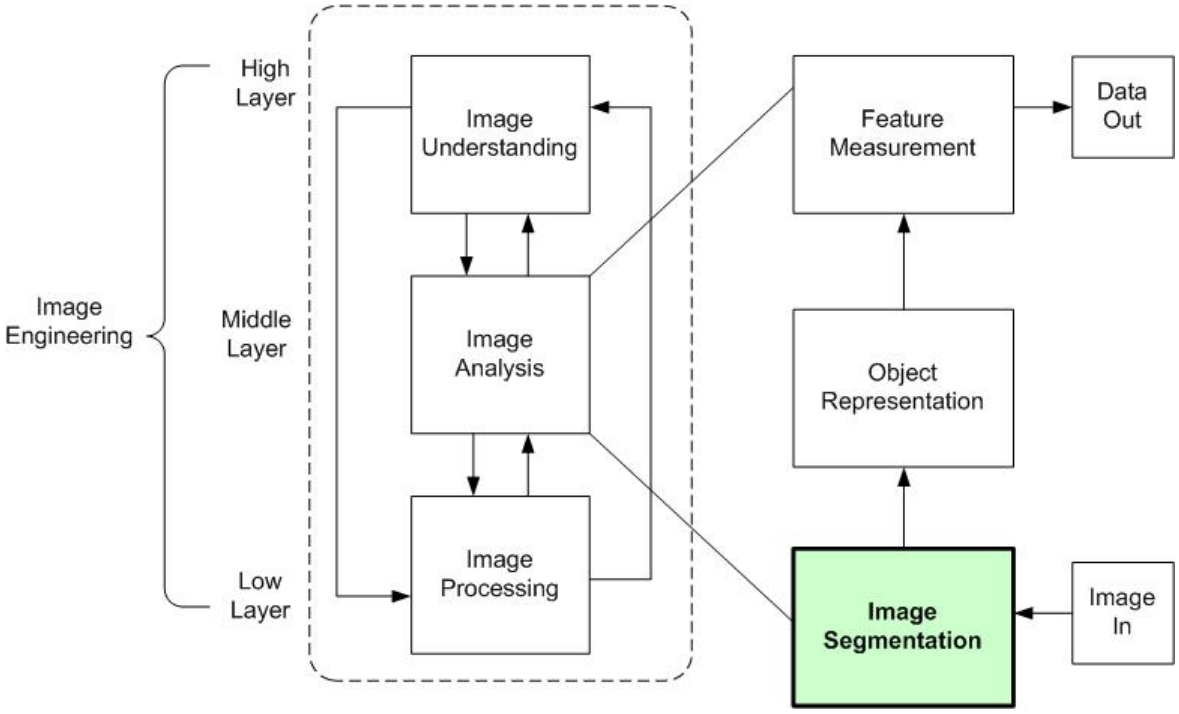

Figure 1.1: Image engineering and image segmentation [1]

1.1 Research Motivations

A good segmentation technique should give accurate results in a reasonable time. Accurate results mean that the segmented regions should be uniform and homogeneous with respect to a certain criteria, such as the intensity. Additionally, these regions must be without many small holes. Finally, adjacent regions should have different values of the chosen criteria. Another important requirement for good segmentation is to be independent on manual intervention.

A good ultrasound image segmentation technique should make use of all prior knowledge such as image features (e.g., intensity) and shape. All methods that proved to be successful are based either implicitly or explicitly on this concept.

Our motivation is to achieve the aforementioned requirements for a good image segmentation, in general, and for a good ultrasound image segmentation, in particular, by applying region growing segmentation technique on ultrasound imaging modality. The proposed segmentation technique is based on some priors to make it more robust.

Many incentives are contributed to the choice of using ultrasound imaging. First, it is a safe means of imaging the human body because it emits no ionizing radiation, and it uses low-power sound waves. Hence, no known long term side effects. Second, it is a quick modality since it can be made in a few minutes. Two other strengths of ultrasound imaging are its rel-

atively low cost and portability. Unfortunately, there are some problems associated with using ultrasound images. The most common problem is the speckle noise, which significantly affects the quality of the segmentation output either manual or computer-aided segmentation. Two other problems are the low contrast and week boundaries. These drawbacks limit working with this modality in image processing in general, and in image segmentation in particular.

In this thesis, we are interested in prostate segmentation in ultrasound images. Prostate segmentation is an essential process because it detects the prostate volumes and boundaries, which both play an important rule in the diagnosis of prostate diseases and treatment. Moreover, in case of prostate cancer, prostate volumes and boundaries are so important in follow up of the cancer, which may help in reducing death rate.

There are many techniques used for prostate segmentation in ultrasound images. The classical techniques do not depend on shape modeling and knowledge of ultrasound images, while recent techniques focus on the incorporation of prior knowledge about shape and speckle [2].

1.2 Objectives

The main objective of this thesis is to design an automated segmentation technique that can meet the requirements of the segmentation process without manual interaction. Additionally, the proposed technique should per-

form well on ultrasound images without needing any preprocessing steps to overcome the speckle noise and the other known artifacts of images. The proposed technique benefits from this speckle noise to achieve automation of the proposed segmentation technique. The proposed technique can be used for routine clinical practice as it is automated, accurate, robust, fast, and simple.

1.3 Thesis Outline

In chapter 2, ultrasound medical imaging basics are discussed. A brief idea about the mechanism of ultrasound imaging and its different modes is given. Also, the advantages and disadvantages of ultrasound imaging are explored. In chapter 3, a survey of the current medical image segmentation techniques is introduced. Chapter 4 presents Fuzzy C-Means (FCM) segmentation technique, which is an automated segmentation technique. FCM is used as a benchmark for evaluating the proposed technique. Chapter 5 introduces the proposed automated modified region growing segmentation technique, where the results for applying the proposed technique to a set of ultrasound images are introduced. Chapter 6 presents the experimental results of three techniques: FCM, the automated conventional region growing, and the automated modified region growing. The accuracies of the three techniques are compared to evaluate the performance of the proposed technique. Finally, the thesis is concluded in chapter 7, summarizing the strengths of the

proposed technique, and outlining our future work to extend the proposed technique.

Chapter 2

ULTRASOUND IMAGING

This chapter tackles the ultrasound imaging modality and explains its mechanism. The different modes of ultrasound are briefly represented. The advantages and disadvantages of this modality are also investigated.

2.1 Ultrasound Preliminaries

Today, the role of medical imaging is not limited to simple visualization and inspection of anatomic structures, but it goes beyond that to patient diagnosis, advanced surgical planning and simulation, radiotherapy planning, etc. Various medical imaging modalities such as ultrasound, X-ray, Computer Tomography (CT), and Magnetic Resonance Imaging (MRI) are widely used in routine clinical practice. Ultrasound is one of the most common medical image modalities, and it is used in nearly all hospitals and clinics. Its distinc-

Figure 2.1: Ultrasound machine [3]

tive feature is that it uses high frequency ultrasound to construct an image rather than the traditional x-ray. It is an imaging technique in which deep structures of the body are visualized by recording the reflections (echoes) of ultrasonic waves directed into the tissues. There are three steps to create an ultrasound image. First, producing a sound wave, then, receiving echoes, and finally, interpreting those echoes. The ultrasonic waves are produced by electrically stimulating a piezoelectric crystal called a transducer. As the beam strikes an interface or boundary between tissues of varying acoustic impedance (e.g., muscle and blood) some of the sound waves are reflected back to the transducer as echoes. The echoes are then converted into electrical pulses that travel to the ultrasonic scanner, where they are processed and transformed into a digital image displayed on the monitor, presenting a picture of the tissues under examination. However, the interference of those echoes, having different phases, add together to give a resultant wave whose amplitude and phase varies randomly resulting in the speckle, which is common in ultrasound images. It should be noted that the speckle is more dependent on the measuring system than on the tissue itself. The speckle is detrimental because it reduces both image contrast (the ability to see the desired object against the background) and the distinction of subtle gradations and boundaries in the tissue structure. A conventional ultrasound imaging device is shown in Fig. 2.1. Frequencies in the range of 2 to 18 MHz are used in diagnostic ultrasonography. The choice of frequency is a trade-off between spatial resolution of the image and imaging depth. The lower frequencies

provide a greater depth of penetration but produce less resolution, while the upper range provide less penetration with high resolution. Ultrasound images are highly detailed and geometrically correct to the first order [4]. There are two basic equations used in ultrasonic imaging [5]. The first equation is

$$d = \frac{1}{2}tc$$

where

d : the one way distance of an object that cause the echo

t : time delay

c: the speed of sound in tissue (between 1450 and 1520 m/s)

The second equation is

$$s(t) = T(t) \otimes B(t) \otimes A(t) \otimes \eta(t)$$

where

S(t): received signal strength

T(t): transmitted signal

B(t): transducer properties

A(t): attenuation of signal path to and from the scatterer

$\eta(t)$: strength of the scatterer

2.2 Ultrasound Modes

Ultrasound modes include A-mode, B-mode, M-mode, and doppler mode.

A-mode is the simplest type of ultrasound, in which a transducer is used to scan a line through the body. The returned echoes are plotted on an oscilloscope as a function of depth.

In B-mode, a linear array of transducers is used to simultaneously scan a plane through the body, and the strength of the returned echoes is displayed as bright spots in their geometrically correct direction and distance. It is displayed as a 2D image.

In M-mode, a rapid images sequence of B-mode scans are displayed on screen to enable doctors to see and measure the range of motion of an organ, whose boundaries produce motion reflections relative to a fixed probe.

Doppler mode is based on the doppler effect. It can be defined as the change in frequency and wavelength of a wave for an object moving relative to the source of the waves [3].

Ultrasound imaging has a lot of strengths that can make it ideal in numerous situations rather than the other modalities. First, ultrasound has a non-radioactive nature, hence, it has no cumulative biological side effects. This feature makes it a non-invasive safe means of creating cross sectional images of the human body. Second, it is a quick modality, since it can be made in a few seconds. Third, it is often small and easily moved as it can be done while standing next to the bed of the patient. This is useful especially when the patient is in intensive care unit, thus, avoiding the danger caused while moving him to the radiology department. Finally, it is relatively inexpensive compared to other modalities. From all the aforementioned advantages,

we can conclude that if there is a diagnostic question to be resolved by any of the medical imaging modalities, ultrasound should be one of the selected choices as it offers the best price-to-performance ratio. Ultrasound is extensively used for obstetric/gynecologic, cardiac, vascular, prostate, breast, and general abdominal imaging. On the other hand, there are characteristic artifacts which make the segmentation process tough such as the inherent presence of speckle noise, attenuation, shadows, and signal dropout due to the orientation dependence of the acquisition which can cause missing boundaries. These artifacts can have negative effects on image interpretation and diagnostic tasks performed by experts or by computerized automated feature detection and extraction techniques. Additionally, these images usually have low contrast and fuzzy boundaries between the organ or the region of interest, to be segmented, and the background. These difficulties make the ultrasound images inherently hard to segment [4].

A lot of efforts have been done over the years for modeling and reducing the speckle noise in ultrasound images using different filters and enhancing techniques. For example, several techniques for suppressing speckle noise have been developed for ultrasound images in [6]-[12]. These efforts achieve good results but consume time, hence, eliminating the advantage of being a fast imaging technique.

Most of ultrasound exams are non-invasive, performed by using a transducer on the skin, however, some of them is done inside the body (invasive ultrasound). In these exams, the transducer is attached to a probe. This

probe is placed into different places in the body such as transesophageal echocardiogram, in which the transducer is inserted into the esophagus to obtain images of the nearby heart. In transvaginal ultrasound, a transducer is inserted into a woman's vagina to view her uterus and ovaries. In transrectal ultrasound (TRUS) imaging, a transducer is inserted into a man's rectum to view his prostate [14]. Since we are interested in prostate segmentation, we only consider TRUS in this thesis, and it is explained in detail in the next section.

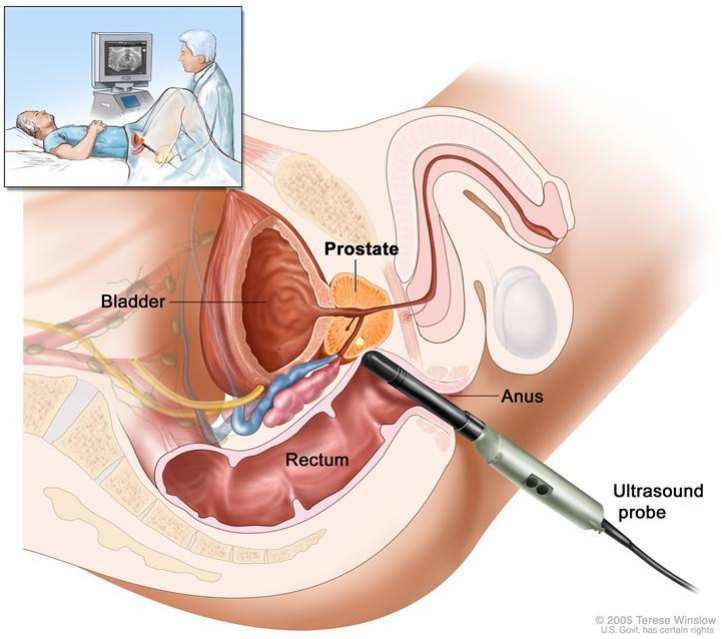

Figure 2.2: Trans-rectal ultrasound (TRUS) [13]

2.3 Trans-Rectal Ultrasound (TRUS) Imaging

Trans-rectal ultrasound (TRUS) imaging is a procedure, in which a probe is inserted into the rectum, as shown in Fig. 2.2. It emits high energy sound waves, which penetrate internal tissues or organs and produce echos. Those echos create an image of organs in the pelvis. Trans-rectal ultrasound (TRUS) images are widely used for the screening of the prostate gland. TRUS images may reveal prostate cancer, benign prostatic hypertrophy, or prostatitis. TRUS images may also be used to help guide a biopsy of the prostate [13].

Chapter 3

STATE-OF-ART MEDICAL IMAGE SEGMENTATION TECHNIQUES

In this chapter, we survey almost all the algorithms that have a generalized scope, which are the basis of most of the segmentation techniques. In addition, the advantages and disadvantages of each technique are discussed.

3.1 Medical Image Segmentation Definition

It has been commonly known that visual interpretation of medical images is highly subjective. Therefore, the need arises for image processing techniques that must be applied on medical images to help the radiologists for

easier and better diseases diagnosis. Image segmentation is the first step and also one of the most critical tasks of image analysis and processing because the segmentation results affect all the subsequent processes of image analysis such as object representation and description, feature measurement, and even the following higher level tasks such as object classification. Hence, image segmentation is the most essential and crucial process for facilitating the delineation, characterization, and visualization of regions of interest. Manual segmentation is not only a tedious and time consuming process, but also it is inaccurate especially with the increasing medical imaging modalities and unmanageable quantity of medical images that need to be examined. Segmentation by experts has shown to be variable up to 20%. It is therefore desirable to use automated algorithms that are accurate and require as little user interaction as possible. In the segmentation process, the anatomical structure or the region of interest needs to be delineated and extracted out so that it can be viewed individually. Generally, image segmentation can be defined as the process of partitioning a digital image into multiple regions (set of pixels). The goal of segmentation is to simplify and/or change the representation of the image into something that is more meaningful and easier to analyze. The result of image segmentation is either a set of regions that collectively cover the entire image or a set of contours extracted from the image [1]. According to this general definition, we can define the medical image segmentation, more specifically, as the process of delineating and separating the anatomical structure (region of interest) so that it can be viewed indi-

vidually in order to achieve important objectives such as patient diagnosis, radio therapy planning, and advanced surgical planning and research.

3.1.1 Mathematical Meaning of Image Segmentation

If the domain of the image is given by I, then, the segmentation problem is to determine the sets whose union is the entire image I. Thus, the sets that make up segmentation must satisfy:

$$I = \bigcup_{k=1}^{K} S_k$$

where $S_k \bigcap S_j = \varnothing \; \forall \; k \neq j$, and each S_k is a connected region. Ideally, segmentation method defines those sets that belong to distinctive anatomical structures or regions of interest in the image.

3.1.2 Hard Segmentation and Soft Segmentation

There are two concepts of segmentation: hard segmentation and soft (fuzzy) segmentation. Hard segmentation is the segmentation that forces a decision of whether a pixel is inside or outside the object. Hard segmentation is based on the concept of a characteristic function, which is simply an indicator function of whether a pixel is inside or outside its corresponding set. For a location $j \in I$, the characteristic function $X_k(j)$ of the set S_k is defined as:

$$X_K(j) = \begin{cases} 1 & if\ j \in S_k \\ 0 & otherwise \end{cases} \tag{3.1}$$

On the other hand, soft (fuzzy) segmentation allows regions to overlap. Soft segmentation is very important in medical image segmentation because of partial volume effects, where multiple tissues contribute to a single pixel resulting in a blurring of intensity across boundaries. Soft segmentation is considered the generalization of the characteristic function in eq. (3.1). This generalization is defined as the membership function which does not have to be binary valued. A membership function $M_k(j)$ should satisfy the following conditions [15]:

$$0 \leq M_k(j) \leq 1 \quad \forall k,\, j$$

$$\sum_{k=1}^{k} M_k(j) = 1 \quad \forall j$$

The general imaging artifacts such as speckle noise, motion, and partial volume effects can significantly affect the outcome of the segmentation process. Hence, in order to guarantee a good segmentation, preprocessing steps should be performed before applying any segmentation algorithm. The major problem faced in medical images is the time consumed in the preprocessing steps. To overcome these problems, different methods and filters such as mean filters and median filters are used for denoising and enhancing

the images. However, filtering process may lead to loss of some important information.

3.2 Overview of Medical Image Segmentation Techniques

There are many segmentation techniques used in medical images depending on the type of tissue, the anatomy of the Region Of Interest (ROI), and the modality being used. With the huge number of the developed techniques, a classification of image segmentation techniques becomes an essential task. Different classifications have been proposed. For example, in [16], segmentation techniques are classified into three generations according to the level of algorithmic complexity which is added by each of them. In this thesis, the classification of the medical image segmentation techniques is performed so that the algorithms in the same class have some common properties. Additionally, the algorithms in different classes show certain distinguishable properties. Hence, all classes together can include all algorithms. The medical image segmentation techniques are classified into three classes [17]:

1. Structural techniques
2. Stochastic techniques
3. Hybrid techniques

The techniques in each class are discussed in detail in the following subsections.

3.2.1 Structural Techniques

The structural techniques use some information about the structure of the region for segmenting it. Different types of structural techniques are discussed in the following subsections.

3.2.1.1 Edge-Detection Techniques

Edge detection is a problem of fundamental importance in image analysis. In typical images, edges characterize object boundaries, therefore, they are useful for segmentation. Edge detection techniques are commonly used for detecting edges in an image to perform segmentation. The classical edge detection techniques usually use the edge detection operators, which are based mainly on the gradation such as Sobel, Robert, and Prewitt edge detectors [18]. Edges are formed at the intersection of two regions with different intensities.

Advantages: Those techniques work very well only on images with good contrast between different regions.

Disadvantages: They detect all the edges. Hence, it is very difficult to find the relation between the edges and the region of interest. In addition, those algorithms are sensitive to noise.

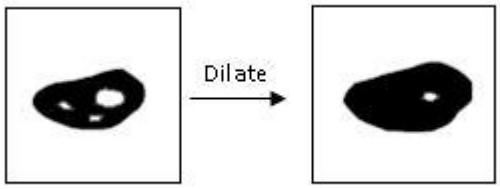

(a) Dilation

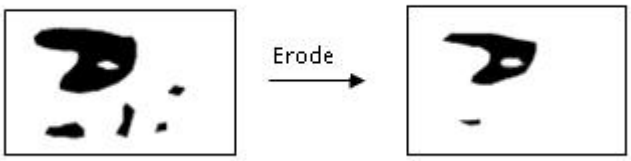

(b) Erosion

Figure 3.1: Morphological techniques [18]

3.2.1.2 Morphological Techniques

Mathematical morphology is widely used in the image processing field. It is based on few simple mathematical concepts from the set theory. Mathematical morphology is a tool for extracting certain components in the image. These components are useful in the representation and description of a region shape such as the boundaries. Morphological techniques are performed by the concept of Structuring Elements (SE). SE is used to scan the whole image, then, the morphological techniques remove the objects that can not fit into the SE. The two most basic operations in mathematical morphology are erosion and dilation. Dilation is used to smooth the boundary by filling the holes and the gaps as shown in Fig. 3.1(a). Erosion is also used for smooth-

ing the boundary but in a different way because it smooths the boundary by removing small-sized objects and fingers of narrow width as indicated in Fig. 3.1(b). Although, morphological techniques are not stand-alone segmentation techniques, we are interested in them because they are widely used in the preprocessing or the postprocessing of the output of the segmentation process.

Advantages: Simple to understand and implement.

Disadvantages: Difficult to control. In addition, those techniques can change the morphology of the input data. It is well known that a series of dilations followed by erode operations leads to loss of high frequencies and fills holes. Similarly, a series of erodes followed by dilations can introduce holes and high frequencies. For the reasons stated above, those algorithms should be avoided when accuracy is of prime concern as there is a risk of losing important data [18].

3.2.1.3 Graph-Searching Algorithms

Graphs are an abstract representation consisting of a set of vertices $V = \{v_1, \cdots, v_n\}$, and a set of edges $E = \{..., \{v_i, v_j\}, ...\}$, where $e_k = \{v_i, v_j\}$ indicates that there is an edge (arc) from vertex i to vertex j. Each edge has an associated weight representing the cost of transition from $v_i$to v_j as shown in Fig. 3.2(a). In these algorithms, edges and surfaces are represented as graphs, and the algorithm tries to find the lowest-cost path, (C_{pq}) indicated in Fig. 3.2(b), between two nodes of the graph using any search algorithm.

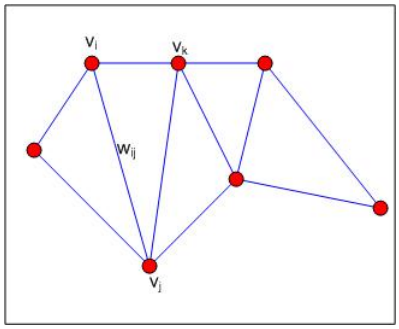

(a) Graph representation

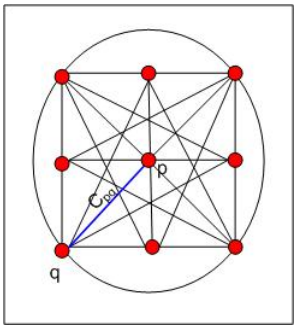

(b) Fully connected graph

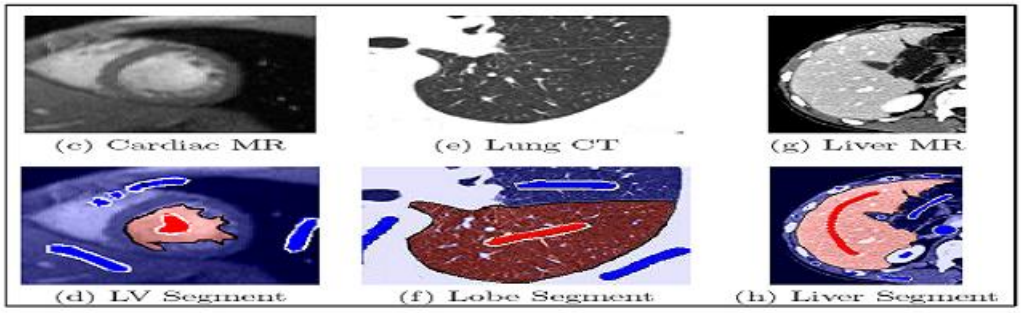

(c) Segmented images using graph search algorithm

Figure 3.2: Graph search algorithm [19]

Advantages: Those algorithms can perform well even if the separations between regions are broken as in the images shown in Fig. 3.2(c).

Disadvantages: Those algorithms require surfaces to be represented as graphs, which could be tricky.

3.2.1.4 Deformable Models

Deformable models are curves or surfaces defined in an image. They are physically motivated model-based techniques for delineating region boundaries by fitting closed parametric curves or surfaces to image data by means of energy minimization. Those models deform under the influence of two basic components of an energy function. The two components are the internal and external forces as indicated in eq. (3.2). The process of deformation is performed by minimizing the energy function $E(c)$ that is designed in such away that its local minimum is obtained at the boundary of the object.

To delineate an object boundary in an image, a closed curve or surface must first be initialized near the desired boundary, and then, it is allowed to deform as shown in Fig. 3.3. Internal forces are defined within the curve or surface to keep it smooth during the deformation. External forces are usually derived from the image to attract the curve or surface towards the desired feature of interest [20].

$$E(c) = \underbrace{\alpha \int_0^1 \mid c'(q) \mid^2 \, dq + \beta \int_0^1 \mid c"(q) \mid^2 \, dq}_{internal\ forces} - \underbrace{\lambda \int_0^1 \mid \nabla f(c(q)) \mid \, dq}_{external\ forces} \quad (3.2)$$

A lot of work is performed on segmentation using 3D deformable surfaces [21]-[24].

Advantages: They have the capability of accommodating the great variability and complexity of biological structures, which is a great advantage in the medical field. In addition, they offer a coherent and consistent mathematical description and they are robust to noise and boundary gaps. Moreover, they offer sub-pixel accuracy for the boundary representation, which may be important to medical applications .

Disadvantages: An important drawback of the snakes is that they require manual interaction to place an initial model or to choose appropriate initial parameters. Besides, they can not be used in non-interactive applications, unless they are initialized close to the structure to be segmented because they are designed as interactive models. Furthermore, the internal energy constraints of snakes can limit their geometric flexibility, and prevent a snake from representing long tube-like shapes or shapes with significant protrusions or bifurcations. Additionally, since classical deformable contour models are parametric and are incapable of adapting topological changes without additional machinery, the topology of the structure of interest must be known in advance. Finally, they are non intrinsic because the energy is

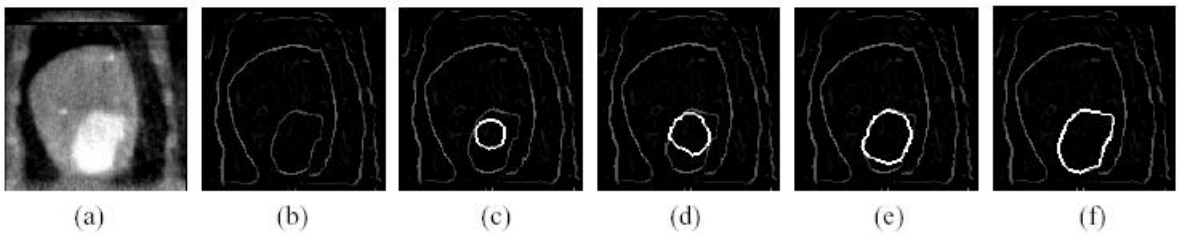

(a) Intensity CT image slice of LV. (b) Edge detected image. (c) Initial snake. (d)-(f) Snake deforming towards LV boundary, driven by "inflation" force.

Figure 3.3: Detecting LV boundary using snakes [25]

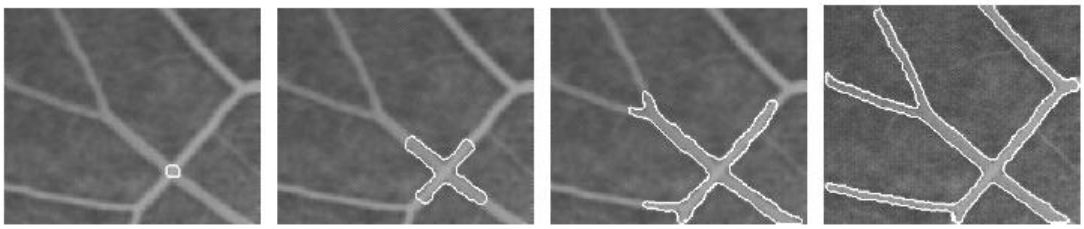

Figure 3.4: Image sequence of clipped angiogram of retina showing an automatically subdividing snake flowing and branching along a vessel [25]

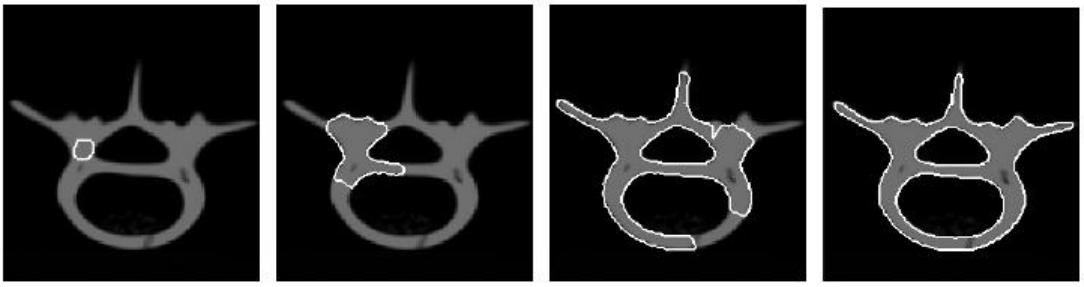

Figure 3.5: Segmentation of a cross sectional image of a human vertebra phantom with a topologically adaptable snake [25]

explicitly dependent on the parametrization of the curve, and it does not have a direct relation with the geometry of the objects [26].

Many improvements have been performed to avoid those disadvantages such as the work involving the development of topology independent shape modeling schemes that allow a deformable contour model to not only represent long tube-like shapes or shapes with bifurcations as shown in Fig. 3.4 but also to dynamically sense and change its topology as indicated in Fig. 3.5.

3.2.1.5 Isosurfaces and Level Sets

Level set models are motivated by the theory of curve evolution, and not by energy minimization like the previous deformable models. Isosurfaces are defined by connecting voxels with intensities equal to the isovalue in a 3D volume. In 3D, it is very tough to follow a surface. Hence, rather than follow the interface itself, the level set approach instead takes the original curve (red one in Fig. 3.6(a)), and build it into a surface. The cone-shaped surface (shown also in Fig. 3.6(b)) has a great property as it intersects the xy plane exactly where the curve sits. This surface is called the level-set function, which takes as input any point on the plane and returns the height of that point. The red curve in Fig. 3.6(a) is called the zero level set because it is the collection of all points that are at height zero [27].

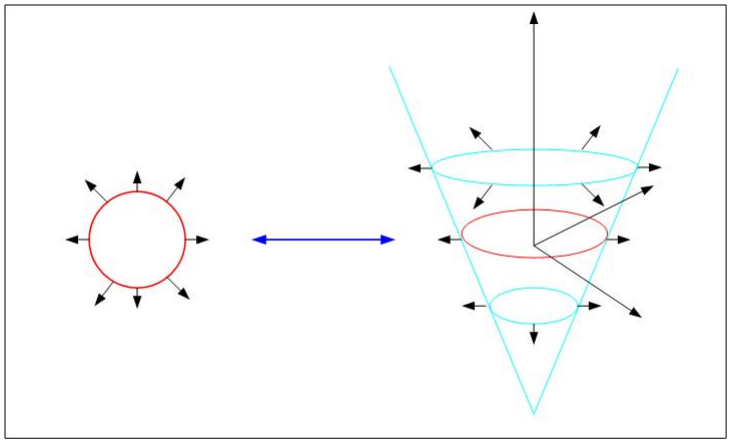

(a) The original front and the level set function

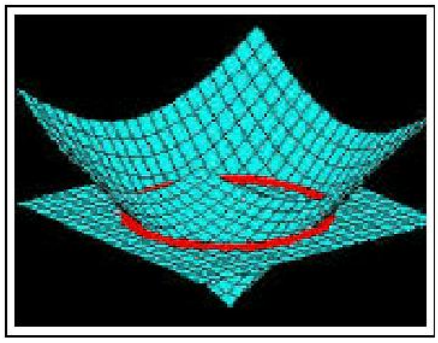

(b) Red curve is zero level set

Figure 3.6: Level set method [27]

A level set is nothing but an isosurface of the function ϕ which implicitly defines hyper-surface S enclosing an image region R such that:

$$S := \partial R$$

To perform segmentation given by S, ϕ is modified rather than modifying S itself. This modification of ϕ can affect the shape of S, and can also change

its topology. S can now break up into disjoint surfaces unlike the definition of S for the deformable surface model. Level set methods are based on a partial differential equation (geometric flow), and can be solved using finite difference methods. The basic equation describing the level set methods is eq. (3.3), which describes the change of ϕ over time (or iteration) t:

$$\phi_t + V.\nabla\phi = 0 \tag{3.3}$$

where

ϕ_t: Temporal partial derivative of level set function.

V: External force field guiding evolution of curve in the image.

$\nabla\phi$: Spatial gradient operator.

If the external force V is defined as the gradient field of an image, the level set methods can be successfully applied for image processing purposes. Then the object is to look for a steady state solution of eq. (3.3), where the surface S has locked onto object edges [28].

Advantages: Level-set models are topologically flexible as they allow automatic changes in the topology. Hence, they can easily represent complicated surface shapes adapting the sudden changes in the biological structures (solving the problem of fixed topology in snakes). Furthermore, these models can incorporate many degrees of freedom, and therefore, can accommodate complex shapes. Several objects can be detected simultaneously without any prior knowledge of their number. Moreover, they are versatile, robust,

accurate, and efficient.

Disadvantages: They require considerable thought in order to construct appropriate velocities for advancing the level set function.

3.2.1.6 Geodesic Active Contours

It is a combination of the active contours and the level set methods, and it is called geodesic active contours. It connects the classical active contours based on energy minimization and geometric level sets based on curve evolution theory.

This technique is based on active contours evolving in time according to intrinsic geometric measures in the image. It means that the boundaries are detected using the active contours based on the geodesic (local) minimal distance computations. Then, assuming this geodesic active contour is introduced at the zero level-set of a 3D function, the computation of the curve is turned to be a geometric flow that is the same as level sets.

However, geodesic active contours are superior than the level sets as they can accurately track boundaries with high variations in their gradient values, including small gaps [29].

The geodesic active contours are based on the concept of minimal surfaces. It is observed that finding S can be put as finding a surface of minimal weighted area with the weight being given by a function $h(f)$ of the image f. Minimization of this area via the calculus of variations leads to a gradient descent rule in image space. This minimization procedure can equivalently be

implemented by finding the steady state solution, i.e., $\phi_t = 0$ of the following partial differential equation:

$$\phi_t = h(f). \mid \nabla\phi \mid . \left(div \frac{\nabla\phi}{\mid \nabla\phi \mid} + v \right) + \nabla h.\nabla\phi \tag{3.4}$$

where

$h(f) = \frac{1}{1+|\nabla G\sigma * f|^2}$

$div\, V = \frac{\partial v_1}{\partial x} + \frac{\partial v_2}{\partial y} + \frac{\partial v_3}{\partial z}$ with $V = \frac{\nabla\phi}{|\nabla\phi|}$

$\nabla G\sigma$: The difference of Gaussian (DoG) filter with size of σ.

V: A constant force in the normal direction to the level sets of ϕ.

By evolving a function ϕ until $\phi_t = 0$ using eq. (3.4). From some initial estimate ϕ_o, one can find a regularized surface S, which is located on edges in the image f [28].

Advantages: It improves the deformable models by making it an intrinsic (geometric) and topology independent as it can change topology during evolution. Also, it improves the existing level sets due to the geodesic formulations. Moreover, it permits simultaneous detection of the internal and external boundaries in many objects without any special procedures for contour tracking. Additionally, it does not need any specific stopping conditions. Finally, it provides unique, stable, and consistent results [29].

3.2.2 Stochastic Techniques

Stochastic techniques are applied on discrete pixels without considering any structural information of the region. These techniques are based only on statistical analysis.

3.2.2.1 Thresholding Approaches

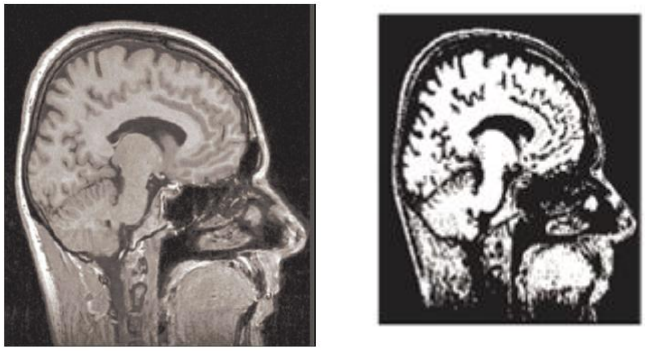

(a) Original image (b) Thresholded image

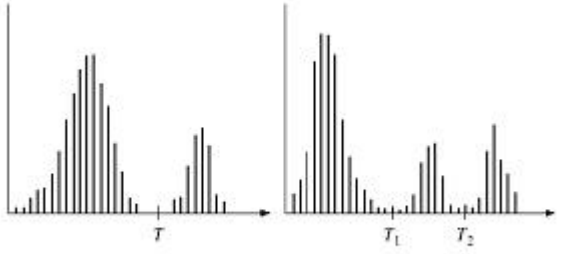

(c) Grey level histogram

Figure 3.7: Thresholding approach [18, 30]

Thresholding approaches segment the image by creating a binary par-

titioning of the image intensities. A thresholding procedure attempts to determine an intensity value called the threshold, which separates the desired classes. The segmentation is then achieved by grouping all pixels with intensity greater than the threshold into one class, and all other pixels into another class. Determination of more than one threshold value is called multithresholding as shown in Fig. 3.7(c).

Advantages: Simple and effective for images having good histogram with good contrast intensities like the image in Fig. 3.7(a), resulting in 3.7 (b).

Disadvantages: It can not be applied to multi-channel images. Besides, it is sensitive to noise and intensity inhomogeneities [18].

3.2.2.2 Classifiers

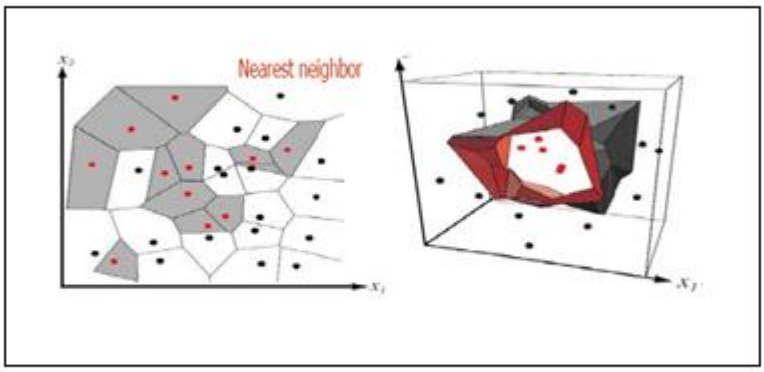

Figure 3.8: Classifiers for 2D and 3D [31]

Classifier methods are pattern recognition techniques that assign to each

pixel in the image a tissue class, where the classes are agreed in advance. Classifiers are known as supervised methods because they require training data that are manually segmented, and then, this training data is used for guiding the automatic segmentation of the new data as shown in Fig. 3.8 for 2D and 3D data. Classifiers can be either parametric or non parametric classifiers as indicated below.

1) Non Parametric Classifiers

Non parametric classifiers are not based on any assumptions about the statistical data structure. Examples of non parametric classifiers include:

- *KNN (K-nearest neighbor) classifier:* Each pixel is classified in the same class as the training datum that has the nearest intensity.
- *Parzen window classifier:* The classification is made according to the majority of the pixels confined within a predefined window of the feature (for example, intensity) centered at the unlabeled pixel intensity.

2) Parametric Classifiers

Parametric classifiers assume that pixels intensities are independent samples from a mixture of probability distributions, usually Gaussian. Bayes classifier is a parametric classifier. It is based on a probabilistic model specification.

Advantages: Classifiers are relatively computationally efficient since there are no iterations, additionally, they can be applied to multi-channel images.

Disadvantages: Classifiers need manual interaction for obtaining training data [32].

3.2.2.3 Clustering Approaches

Clustering can be loosely defined as the process of organizing objects into groups, whose members are similar in some way. In this case, these "objects" are the data pixels, and the "groups" are the clusters. Similar "properties" could be any property the data pixel possesses like the intensity, gradient, and/or color. The cluster is therefore a collection of objects which are "similar" between them and are "dissimilar" to the objects belonging to other clusters. Clustering algorithms essentially perform the same function as the classifier methods without the use of training data. Thus, they are termed unsupervised methods. Two commonly used clustering algorithms are the K-means or ISODATA algorithm, and the fuzzy c-means algorithm (FCM). K-means starts by partitioning the input pixels into k initial clusters. It then calculates the mean pixel, or centroid, of each cluster. It constructs a new partition by associating each point with the closest centroid. Then, the centroids are recalculated for the new clusters, and the algorithm is repeated by alternate application of these two steps until convergence, which is obtained when the pixels no longer switch clusters (or alternatively centroids are no longer changed), is reached. In FCM, each pixel has a degree of belonging to a number of clusters, as in the fuzzy logic, rather than belonging completely to just one cluster, which is the case in K-means. Thus, pixels on the edge

of a cluster, may be in the cluster to a lesser degree than pixels in the center of cluster. In other words, FCM allows labels to be "fuzzy," that is, a pixel can be partially in one cluster and partially in others. FCM also provides information on how well a pixel "fits" a cluster. Since in clustering techniques there is no need for training data, they are termed as unsupervised techniques [33].

Advantages: They don not need training data because they iterate between segmenting the image and characterizing the properties of each cluster.

Disadvantages: Sensitive to noise and intensity inhomogeneities.

3.2.2.4 Markov Random Field Models

Markov Random Field (MRF) is a statistical model, and not a stand-alone segmentation method. However, it is commonly used in segmentation techniques. In medical imaging, MRF is typically used as it considers that only neighboring labels have direct interactions with each other. MRFs are often associated with clustering segmentation algorithms such as the K-means algorithm, or FCM algorithm to incorporate spatial constraints [34].

Advantages: MRF is robust to noise, which makes it widely used in modeling both segmentation classes and intensity inhomogeneities that can occur in MR images.

Disadvantages: The proper selection of the parameters controlling the strength of spatial interactions is challenging. Also, it requires computationally intensive algorithms.

3.2.3 Hybrid Approaches

Hybrid approaches include those techniques which possess characteristics of both structural and stochastic techniques.

3.2.3.1 Region Growing

Region growing is a technique for extracting a region of the image that is connected based on some predefined criteria. These criteria can be based on intensity information. In its simplest form, region growing requires a seed point that is manually selected by an operator.

Advantages: Region growing approach is simple.

Disadvantages: It requires a seed point, which generally means manual interaction. Thus, for each region to be segmented, a seed point is needed [18].

3.2.3.2 Split and Merge

Split and merge technique is the opposite of the region growing. It works on the whole image. Also, it requires the input data to be organized into a pyramidal grid structure of regions, with each region organized in groups of four in case of 2D, and of eight in case of 3D. Any region can be split into subregions, and the appropriate regions can be merged into a single larger region.

Advantages: No manual interaction.

Disadvantages: It requires the input to be organized into a pyramidal grid structure which could be difficult [17].

3.2.3.3 Atlas-Guided Approaches

Atlas-guided approaches are good candidates for medical image segmentation when a standard atlas, such as these models shown in Fig. 3.9(a), (b) [35], is available. First, the atlas is performed by compiling information on the anatomy that requires segmentation. Then, it is used as a guide for segmenting new images. In order for atlas to guide the segmentation, it has to be aligned to the patient's space. In [36], the atlas, a set of MRIs taken on a template subject, is aligned to the patient by registering the template MRIs to the MR scans of the patient, using a non-rigid registration algorithm. This process results in a correspondence field, which maps each pixel in the atlas space to one in the patient coordinate system. The spatial priors are then applied to correspondence field resulting in patient specific spatial priors, which guide the segmentation as indicated in Fig. 3.9(c).

Advantages: The labels are transferred as well as the segmentation.

Disadvantages: The approaches are best suited for segmenting stable structures, hence, accurate segmentation of complex structures is very difficult due to anatomical variability.

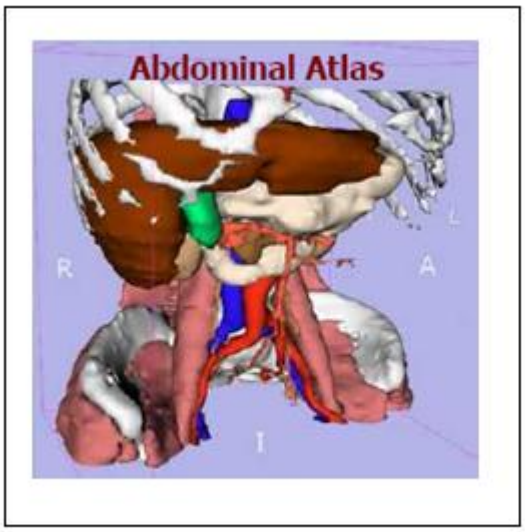

(a) Abdominal atlas

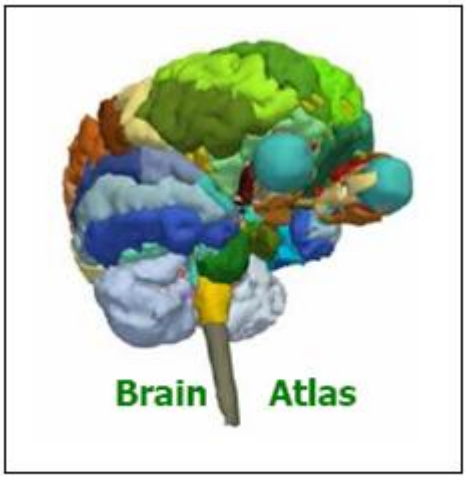

(b) Brain atlas

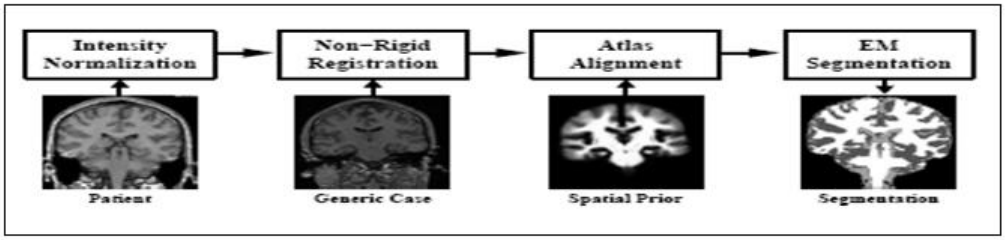

(c) Segmentation using atlas guided approach

Figure 3.9: Atlas-guided approach [35, 36]

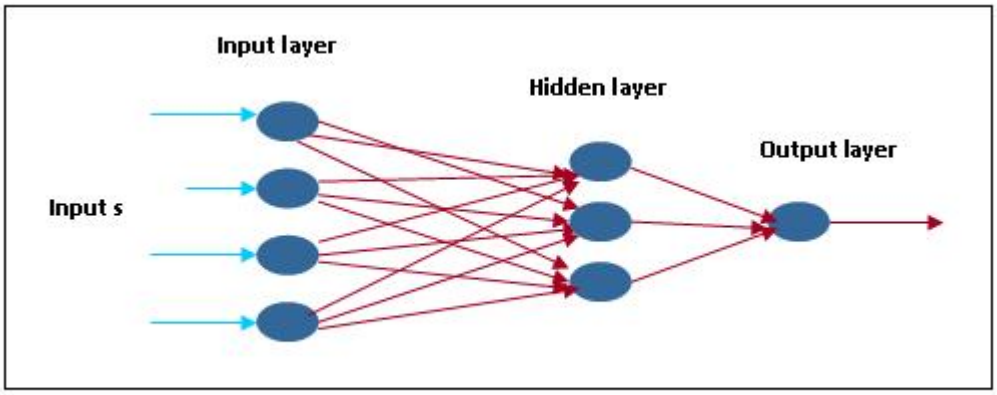

Figure 3.10: Artificial neural network [37]

3.2.3.4 Artificial Neural Networks (ANN)

ANNs are massive networks of parallel and distributed computational elements called neurons, as shown in Fig. 3.10. These neurons are tied together with weighted connections to achieve learning through the adaptation of these weights. It simulates the function of the human brain. ANNs can be used in a variety of ways for image segmentation, either as classifiers by determining the weights using training data in an supervised technique or as a clustering method in an unsupervised technique.

Advantages: Partially overcomes the drawbacks of the conventional segmentation algorithms based on structural knowledge, which often require considerable user expertise. In addition, spatial information can be easily incorporated into its classification procedures due to the large number of highly interconnected and tied processing elements.

Disadvantages: Their processing is usually performed on a standard serial computer, hence, reducing its potential computational advantage of being inherently parallel [37].

3.2.3.5 Watershed Approaches

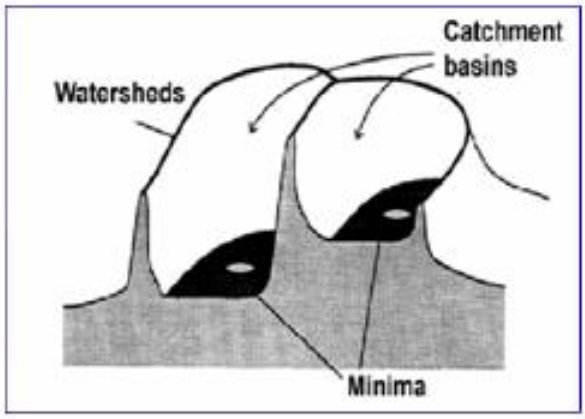

(a) The immersion analogy

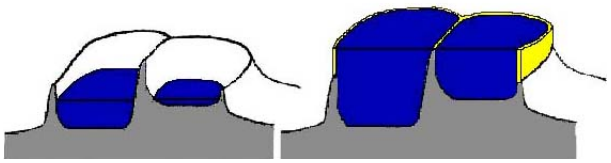

(b) Dam construction

Figure 3.11: Watershed approach [38]

The watershed algorithm depends on the idea of mathematical morphology to divide images into homogeneous regions. It deals with the image as topographical surface, where the gray levels represent altitudes. According

to this concept, there are three types of points:

- Points belonging to a regional minimum.
- Points at which a drop of water would fall to a single minimum (the catchment basin).
- Points at which a drop of water would be equally likely to fall to more than one minimum (watersheds) as shown in Fig. 3.11(a).

Main idea: Assume that there is a hole punched in each regional minimum, and that the entire topography is flooded from below by letting water rise through the holes at a uniform rate. When rising water in distinct catchments basins is about to merge, a dam is constructed to stop this merging. These dam boundaries are the watershed lines. This is shown in Fig. 3.11(b)[18].

Watershed segmentation algorithm:

- Start with all pixels that have the lowest possible value. These form the basis for initial watersheds.
- For each intensity level k:
- For each group of pixels of intensity k:
- If adjacent to exactly one existing region, add these pixels to that region.
- Else if adjacent to more than one existing regions, mark as boundary.

- Else start a new region.

Advantages: It is an intuitive and easy method. Additionally, it introduces closed lines around regions every time.

Disadvantages: This method has the common problem of oversegmentation that occurs when the image is segmented into an unnecessarily large number of regions. Therefore, in case of medical imaging, watershed algorithms are usually followed by a postprocessing step to merge the separated regions that have the same structure [39].

3.3 Conclusion

From the survey conducted above, we can conclude that there is a large number of techniques used for medical image segmentation. The concept of each technique is explained in details. Also, the advantages and disadvantages of each technique are explored. It should be noted that some of the techniques suffer from the manual interaction problem. This interaction is necessary in order to initialize the segmentation process. Examples of these techniques are deformable models, classifiers, and region growing.

On the other hand, there are other techniques that are automatic techniques. These techniques do not need any manual interaction for initializing segmentation such as split and merge, watershed, and Fuzzy C-Means (FCM) clustering.

In this thesis, the work is focused on two segmentation techniques among

these techniques: the region growing technique, and the Fuzzy C-means (FCM) clustering technique.

Chapter 4

FUZZY C-MEANS CLUSTERING (FCM)

TRUS images do not have strong boundaries (fuzzy) between organs, or ROIs, and the surrounding tissues. The segmentation of TRUS images is known as fuzzy segmentation, where each pixel is assigned a membership value in each region. More accurate estimates of region properties are usually obtained, when taking into account the memberships while computing these properties. FCM is one of the techniques that are used to obtain such classification. In this chapter, we present Fuzzy C-Means (FCM) segmentation technique. FCM performs the segmentation without manual interaction, as discussed in chapter 3. Since FCM is widely used in automatic medical image segmentation [40]-[42], it is selected as a benchmark in this thesis.

4.1 FCM Concept

FCM, in particular, is used to obtain segmentation via fuzzy pixel classification. Unlike hard classification methods, which force pixels to belong exclusively to one class, FCM allows pixels to belong to multiple classes with varying degrees of membership. This approach allows additional flexibility, making it more suitable for the medical image segmentation. FCM is an unsupervised technique, which clusters data by iteratively computing a fuzzy membership function and a mean value estimates for each cluster. The fuzzy membership function, whose values must be between 0 and 1, shows the degree of similarity between the data value at that location and the prototypical data value, or centroid, of its cluster [43].

Mathematically, the FCM algorithm for scalar data seeks the membership functions μc_i and the centroids v_i, such that the following objective function is minimized:

$$J_m(P,V) = \sum_{i=1}^{k} \sum_{x \in c_i} (\mu c_i(x))^m |x - v_i|^2 \quad \forall x \in X \tag{4.1}$$

where P is the fuzzy partitioning of the data set X formed by $c_1, c_2, \cdots, c_k$. The parameter m is a weight that determines the degree to which partial members of a cluster affect the clustering result. m is the weighting exponent on each fuzzy membership, the larger the value of m, the fuzzier the partition. It is well-known that choosing $m = 2$ is a good value. This value for m has the advantage of simplifying the update equations, and can

therefore speed up computer implementations of the algorithm. The FCM algorithm tries to minimize J_m by iteratively updating the partition matrix using the following equations:

$$\mu c_i(x) = \frac{1}{\sum_{j=1}^{k} \left(\frac{|x-v_i|^2}{|x-v_j|^2} \right)^{\frac{1}{m-1}}} \quad \forall 1 \leq i \leq k,\ x \in X,\ m > 1 \tag{4.2}$$

$$v_i = \frac{\sum_{x \in X} (\mu c_i(x))^m x}{\sum_{i=1}^{k} (\mu c_i(x))^m} \tag{4.3}$$

The FCM objective function is minimized when high membership values are assigned to pixels whose intensities are close to the centroid for its particular cluster, and low membership values are assigned when the pixel data is far from the centroid. In the last decades, FCM has been widely used in medical image segmentation especially with the advantage of being unsupervised technique. But, less report on FCM usage for ultrasound images segmentation because it is not robust for ultrasound images, which are usually corrupted by noise. However, many works used FCM for the segmentation of ultrasound images, but first, they had to do preprocessing steps for enhancing the ultrasound images and remove noise. For example, in [40], FCM preprocessing is performed by using histogram equalization and median filter. Besides FCM itself is a time-consuming technique due to the iterations it performs, the time consumed for the preprocessing steps used for enhancing adds extra

time to the FCM process.

We use FCM in the segmentation of the prostate on ultrasound images in order to compare it as an operator independent technique, with the proposed technique to measure its quality. In this chapter, the performance and the results of FCM technique is examined.

4.2 FCM Implementation

FCM is implemented according to the following algorithm:

FCM algorithm FCM(X, c, m, e) , where

X: Unlabeled data set.

c: The number of clusters.

m: A weighting value in the objective function.

e: A threshold for the convergence criteria.

1) Initialize prototype $V = v_1, v_2, \cdots, v_c$.

2) Repeat $V^{Previous} \longleftarrow V$

3) Compute membership functions using eq. (4.2).

4) Update the prototype, v_i in V using eq. (4.3). Until

$$\sum_{i=1}^{c} |v_i^{Previous} - v_i| \leq e \tag{4.4}$$

The process starts by choosing the number of output clusters c, which is selected according to the image under consideration. Then, initializing the

prototype v with random values, and computing the membership function according to eq. (4.2). The next step is to update the prototype v. The process is iterated till the condition of eq. (4.4) is met. This condition is verified when the difference in the prototype values is less than a certain threshold, e, which is chosen to be 0.05. After the previous condition is met, the membership function of each pixel in the image is examined to determine the cluster to which it belongs. The criterion used is that if the membership function ($\mu c_i(x)$) of a pixel is greater than or equal to 0.8, then, this pixel belongs to the cluster.

4.3 Results

In this section, we present the results of applying FCM technique on a set of biomedical TRUS prostate images without performing any preprocessing steps to enhance the images. The implementation of FCM is done using MATLAB 7, running on a machine with Intel Centrino Core2Duo 2 GHz processor. FCM starts with no manual interaction. Figs. 4.1-4.5(a) show the original TRUS prostate images. Figs. 4.1-4.5(b), show that results of using the FCM segmentation. It can be seen that FCM segments the prostate inaccurately due to the speckle noise that is inherently present in ultrasound image. FCM could not handle this noise because it appends all pixels with membership values satisfying the above criterion to the prostate cluster. The binary prostate cluster for each image is shown in Figs. 4.1-4.5(c), while the

gold standard of these images is shown in Figs. 4.1-4.5(d). The difference between the gold standard of each image and the prostate binary cluster is introduced in Figs. 4.1-4.5(e). From this difference, it can be seen that FCM has poor performance in TRUS prostate images.

4.4 Conclusion

In terms of programming implementation, FCM is relatively straightforward. It employs an objective function that is intuitive and easy-to-grasp. However, from the previous results, it is clear that FCM technique gives unsatisfactory segmentation results. It fails to achieve the requirements of a good segmentation due to the following reasons. First, its accuracy is sensitive to the speckle noise in ultrasound images as it squares the "error" between a prototype and a pixel, thus, the effect of noisy pixels is emphasized. Second, it gives counter-intuitive membership values for noisy pixels, which should not receive significant memberships with any of the clusters. We surprisingly, found that FCM gives them membership values close to those of the pixels in the prostate cluster. This results in the inaccurate segmentation results shown above. Hence, we can conclude that FCM gives accurate segmentation results only for data sets composed of well-separated clusters, which is not always the case in medical images. In other words, the images to be segmented using FCM, must undergo a series of enhancing techniques to remove the noise, so that FCM can give accurate results [40]. In this thesis, we did

not use any of these enhancing techniques before applying FCM, in order to make a fair comparison with the proposed technique. Moreover, FCM consumes time, which may not be acceptable in critical medical applications.

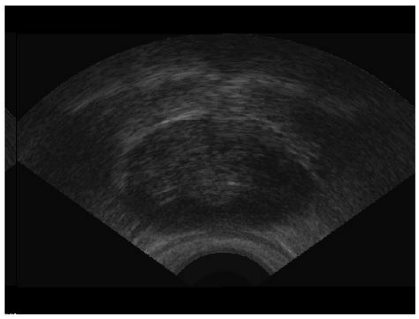

(a) Original image

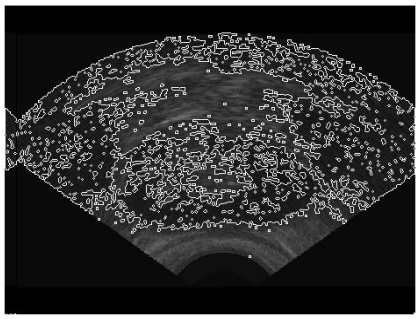

(b) Segmeted prostate

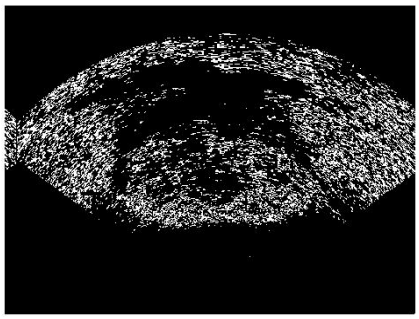

(c) Binary prostate cluster

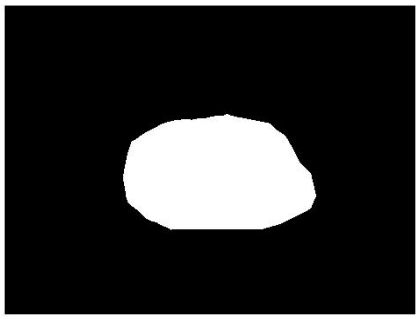

(d) Gold standard

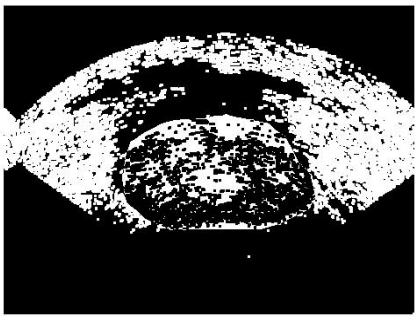

(e) Difference between binary prostate cluster and gold standard

Figure 4.1: FCM results for image 1

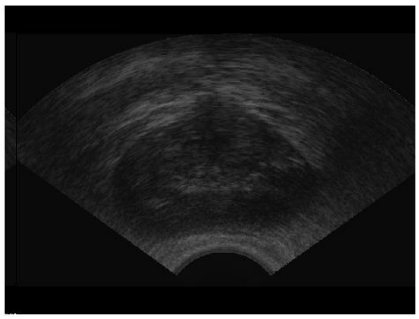

(a) Original image

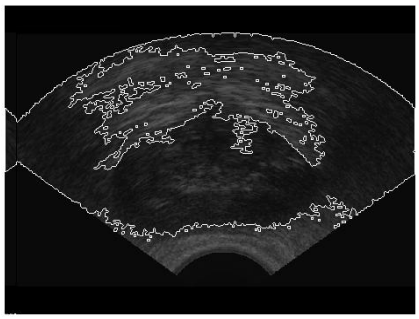

(b) Segmented prostate

(c) Binary prostate cluster

(d) Gold standard

(e) Difference between binary prostate cluster and gold standard

Figure 4.2: FCM results for image 2

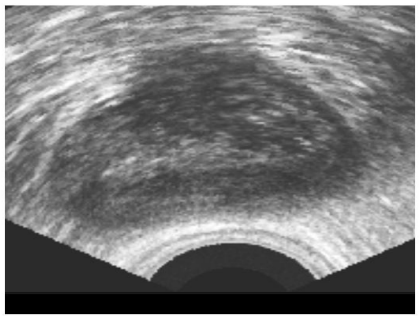

(a) Original image

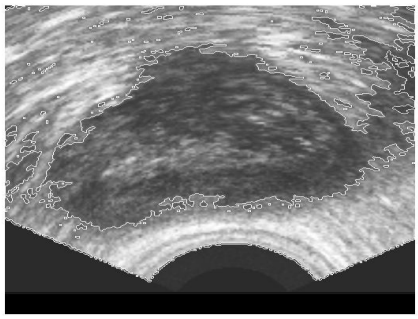

(b) Segmented prostate

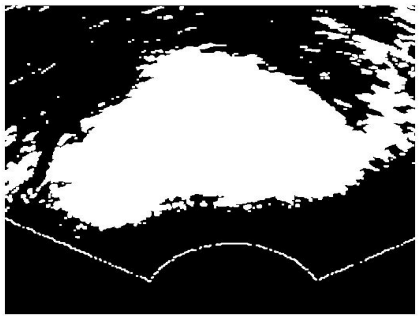

(c) Binary prostate cluster

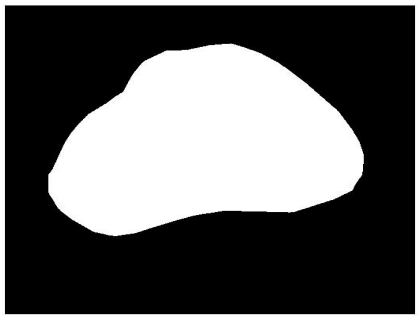

(d) Gold standard

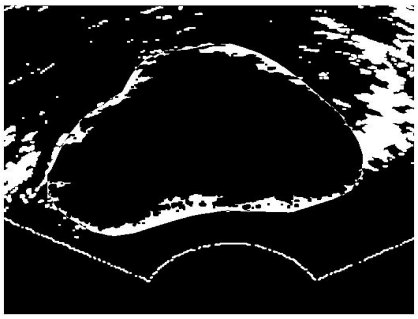

(e) Difference between segmented prostate and gold standard

Figure 4.3: FCM results for image 3

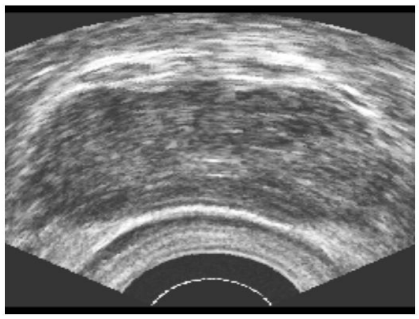

(a) Original image

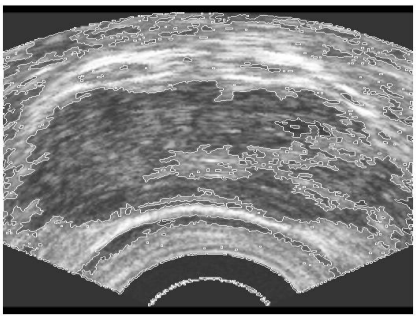

(b) Segmented prostate

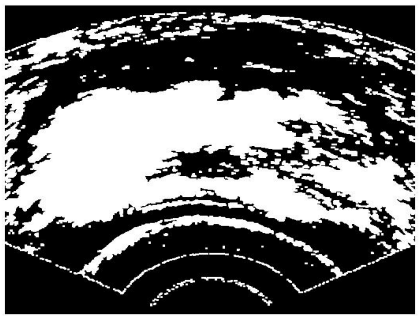

(c) Binary prostate cluster

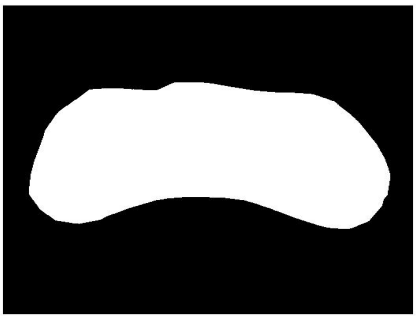

(d) Gold standard

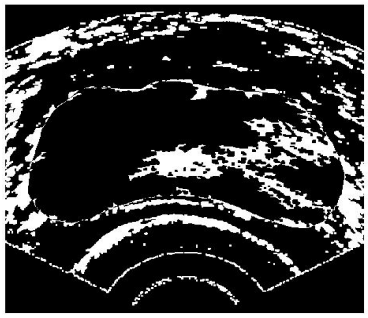

(e) Difference between segmented binary and gold standard

Figure 4.4: FCM results for image 4

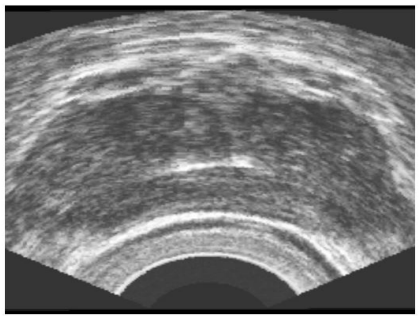

(a) Original image

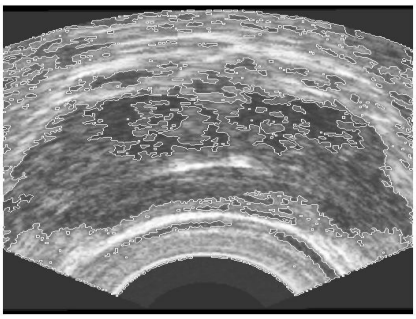

(b) Segmented prostate

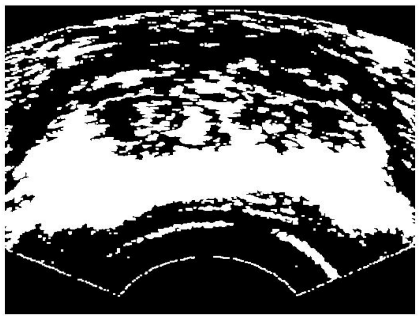

(c) Binary prostate cluster

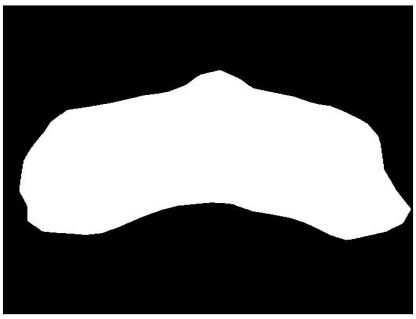

(d) Gold standard

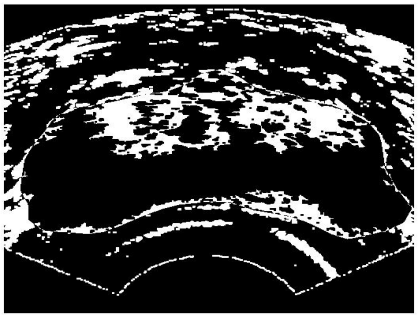

(e) Difference between segmented binary and gold standard

Figure 4.5: FCM results for image 5

Chapter 5

THE PROPOSED AUTOMATED REGION GROWING SEGMENTATION TECHNIQUE

In this chapter, the proposed automated region growing technique is presented. The main goal of the proposed method is to automatically segment the prostate in TRUS images. The proposed automated method is robust, relatively fast, accurate, and simple.

5.1 Conventional Region Growing

In the region growing technique, segmentation is performed by aggregating pixels or subregions into larger regions according to predefined criteria. The

(a) Ideal image

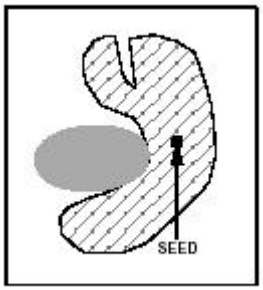

(b) The region of interest is segmented based on a selected seed point

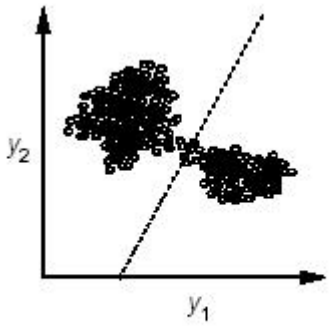

(c) Spearation of pixels with different intensities based on the inensity of the seed point

Figure 5.1: Region growing technique [15]

selection of similarity criteria relies on the problem to be solved and the type of available image data. This similarity criteria can be intensity, color, texture, shape, or size. The region growing process starts with a seed point, which is manually selected. After that, the region grows by annexing to the seed point those neighboring pixels that show similarity in a certain criteria, such as intensity. The process is iterated till it meets a stopping rule. Generally, the region growing should stop, when no more pixels satisfy the criteria for inclusion in that region. This is depicted in Fig.5.1(b)-(c), where the region growing technique has been used to isolate one of the structures from the original image shown in Fig. 5.1(a). Region growing technique offers several advantages over conventional segmentation techniques. It is fast, simple, and easy to implement. However, since the starting seed point must be manually selected in the region growing technique, it suffers from the manual initialization problem. The success of region growing technique depends on the proper selection of this seed point. This results in a main disadvantage for the region growing technique, since the manual interaction is usually debated [18].

5.2 Automated Modified Region Growing Technique

In this thesis, we propose a novel modified region growing technique to segment the prostate in TRUS images. The proposed technique is simple, fast,

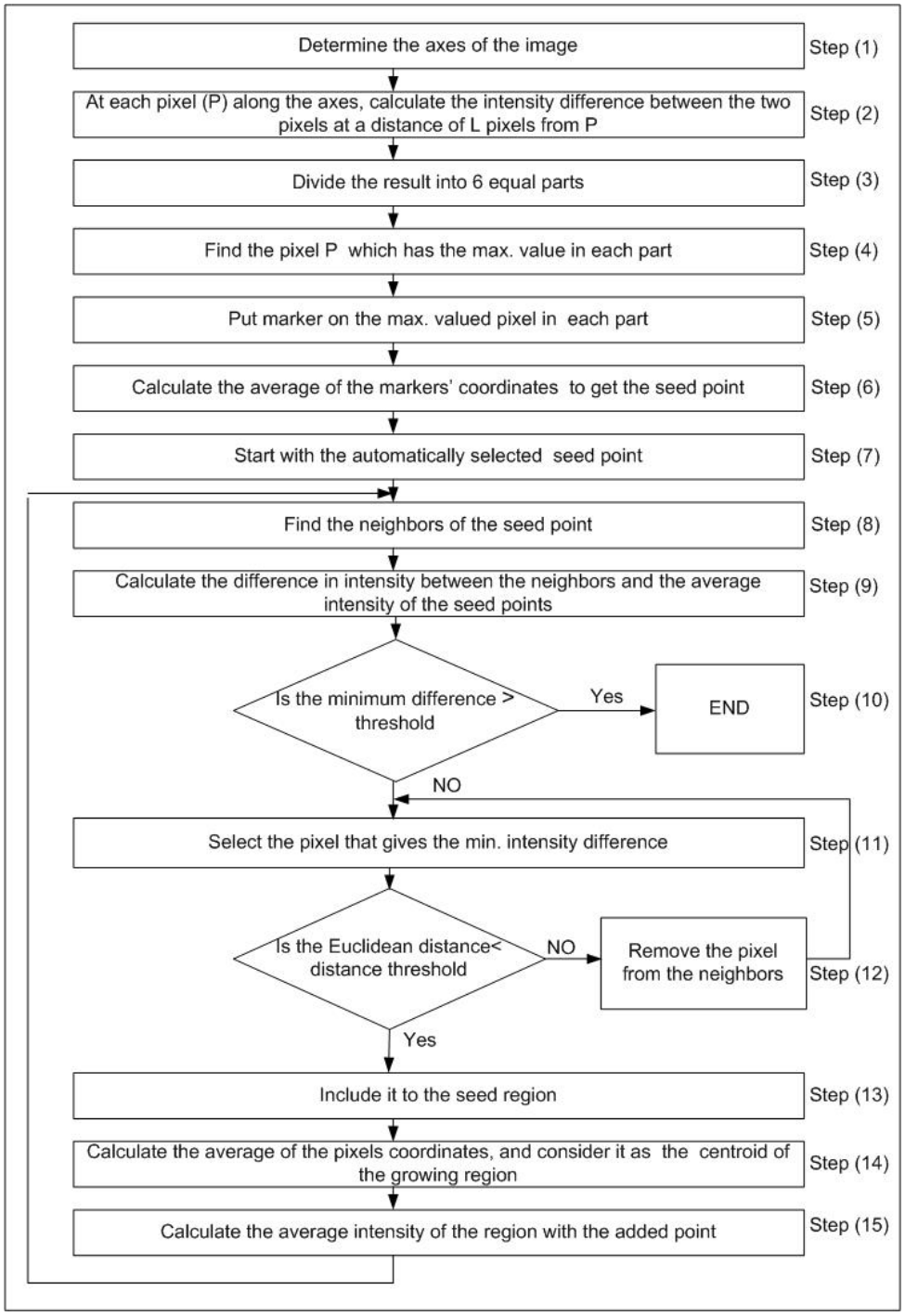

Figure 5.2: Automated modified region growing flow chart

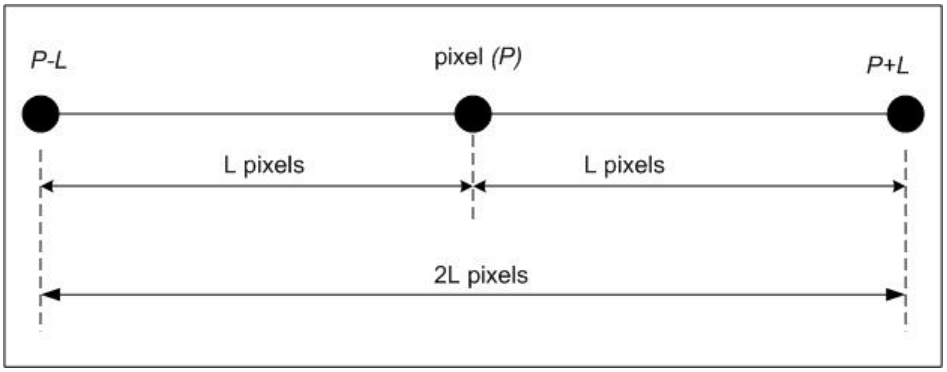

Figure 5.3: Intensity computation procedure

automated, and accurate. The proposed technique not only overcomes the manual interaction problem, but also, makes the region growing technique more robust to noise by considering a controlling parameter, which is the Euclidean distance, while performing the region growing. The main idea of the proposed technique is to make use of the spatial characteristics of the prostate TRUS image, where the size of the prostate is relatively large compared to the scan range of the ultrasound transducer. Hence, there is a high probability that the axes at the centers of the TRUS images traverse through the prostate. The proposed technique is summarized in the flow chart shown in Fig. 5.2, and its details are as follows:

- *Step(1):* Determine the axes of the image;
- S*tep(2)*: At each pixel P along the image axes, we calculate the intensity difference between the two pixels at distances of L pixels from P along the same axis, where we selected $L = 80$ pixels. In other words, we calculate the intensity difference between two pixels separated by

$2L$ pixels and put the result to the pixel P centered between those two pixels as shown in Fig. 5.3. The reason behind that separation is to benefit from the abrupt intensity transition between the prostate area and the noisy background to detect the boundaries between the prostate area and the surrounding noisy areas. It is interesting to mention that in this step, we made use of the characteristic speckle noise in TRUS, instead of considering it as noise and trying to remove it. Also, it should be noted that we have tried the conventional gradient method; however, it could not handle the speckle around the prostate causing failure of this method as it will be discussed in the next section;

- *Step(3):* The image is broken up into 2×3 non-overlapping equal parts;
- *Step(4), step(5):* In each part, the pixel that has the maximum intensity difference is marked. These markers are guaranteed to be located inside the prostate itself or at least surrounding the prostate area.
- *Step(6):* These markers are then used to obtain the seed point, where its indices are calculated as the average of the resulted markers' indices. In this way, the automation of selecting the seed point is achieved.
- *Step(7):* The region growing process starts automatically with the seed point as the initial region to be grown, where the intensity of the seed point is set as the initial intensity mean of the growing region. Moreover, the coordinates of the seed point are used as the initial centroid of the growing region;

- *Step(8):* The neighbors of the selected point, which is initially the seed point, are chosen based on their spatial locations with respect to the selected point;

- *Step(9):* The intensity difference between the selected point and its neighbors is calculated and compared to a small valued threshold;

- *Step(10):* Check if the minimum intensity difference is greater than the intensity threshold. If yes, then, END. If no, then, go to the next step;

- *Step(11):* Select the neighboring pixel that gives the minimum intensity difference;

- *Step(12):* In this step, we overcome the ultrasound images noisy background by introducing a new controlling spatial parameter, which is the Euclidean distance between the centroid of the region to be grown and the pixel to be appended to the region as follows. Check if the Euclidean distance between the pixel that gives the minimum intensity difference and the centroid of the growing region is less than a predefined Euclidean threshold, if no then, remove that pixel from the neighboring list so that it is not selected again and, return to *step (11)*. If yes then, go to the next step;

- *Step(13):* The pixel that satisfies the conditions in *step (10)* and *step (12)*, which are the intensity difference and the Euclidean distance, respectively, is appended to the growing region;

- *Step(14):* After a new pixel is added to the region, calculate the average of the coordinates of the pixels in the growing region, and set it as the coordinates of the new centroid of the growing region;

- *Step(15):* After a new pixel is added to the region, the intensity mean of the region is calculated, and it is considered as the new region intensity mean. Finally, go back to *step (8)*.

5.2.1 Discussion

These steps verify all the goals of a good segmentation for the following reasons. First and foremost, accurate because the obtained seed point is guaranteed to be inside the organ, which is necessary to get accurate segmentation. Second, they are robust as they could handle the noise problem successfully, using the modification of the Euclidean distance. Third, they achieve high performance speed.

5.3 Results

The implementation of the proposed method is done using MATLAB 7. The proposed technique is tested on a set of thirty biomedical ultrasound images. The implementation is performed on a machine with Intel Centrino Core2Duo 2GHz processor.

In the following subsections, we introduce the results of combining the automatic selection of the seed point with the conventional region growing

technique, and with the modified region growing technique, respectively.

5.3.1 The Automatic Seed Point Selection Combined With The Conventional Region Growing Technique

The region growing is performed starting with the automatically selected seed point, and the region grows based on the intensity difference between the seed region and the neighbors. The process stops when the minimum intensity difference is greater than a predefined threshold. This is the conventional procedure of the region growing except for the automatic initialization. However, this technique did not give good results for noisy ultrasound images as those shown in Figs. 5.4-5.8(a). Figs. 5.4-5.8(b) show the markers that are chosen based on the intensity feature of the images. Also these figures show the automatically selected seed point, which is obtained by averaging the coordinates of these markers. It can be seen that the proposed automation method succeeds in obtaining a seed point inside the prostate area in all cases. The resulted binary segmented prostates based are shown in Figs. 5.4-5.8(c). The final segmentation result in Figs. 5.4-5.8(d) shows that the prostate in these images is delineated in an inaccurate way. It includes the pixels that have similar intensities, however, they are not in the prostate. The differences between the gold standards, given in Figs. 5.4-5.8(e), and these inaccurate segmentation results are shown in Figs. 5.4-5.8(f).

This method gives reasonable results with accepted accuracies for less

noisy images or the pre-enhanced images. However, in case of very noisy images with no preprocessing for enhancing the image quality and removing noise, like our case, it does not provide an exact delineation of the prostate, and its performance is greatly degraded.

5.3.2 The Automatic Seed Point Selection Combined With Modified Region Growing Technique

According to the results obtained above, the main concern then is to overcome the noise problem in the raw ultrasound images that causes inaccurate segmentation. In order to get accurate segmentation results, it is necessary to include a controlling parameter to hinder the growing region from picking the pixels of the noisy background. In this modified technique, we select the controlling parameter to be the spatial Euclidean distance as explained in details in section 5.2 (*step12*).

We apply this modified technique on the same ultrasound images shown in Figs. 5.9-5.13(a). Also, we use the same technique for selecting the markers that are averaged to obtain the seed point as shown in Figs. 5.9-5.13(b). Region growing is performed considering the Euclidean distance between each pixel, that verifies the intensity requirement, and the centroid of the growing region. This Euclidean distance should be less than a predefined Euclidean threshold. The modified technique achieves better results compared to the results of the conventional region growing technique previously discussed.

The binary segmented prostates are shown in Figs. 5.9-5.13(c). The final segmented prostates shown in Figs. 5.9-5.13(d) indicate how accurately the prostate is delineated without any effect of the noisy background. These results prove that the modified region growing technique is efficient and robust to noise. Also, the difference between the gold standards, shown in Figs. 5.9-5.13(e), and the binary cluster is shown in Figs. 5.9-5.13(f). The obtained result introduce higher accuracies than the previous automated conventional technique.

5.4 Conclusion

The goal of this work is to develop an automatic robust segmentation technique for the prostate in ultrasound images. The above results show that the new method is a very powerful segmentation method. In addition, it gives an automatic prostate segmentation without any manual interaction for the initialization. Moreover, it is a robust technique since it overcomes the common speckle noise problems usually present in ultrasound images by taking into account the spatial Euclidean distance while performing the region growing. Moreover, the segmentation is performed relatively fast, when compared to manual segmentation or other automatic techniques, like FCM discussed in chapter 4, making this technique suitable for routine clinical use for the diagnosis and treatment procedures in prostate diseases.

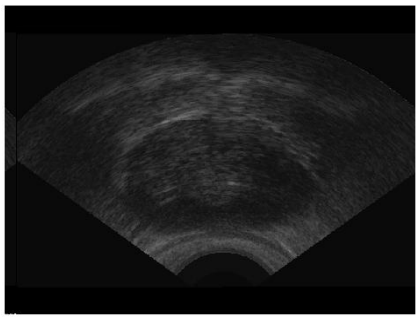

(a) Original image

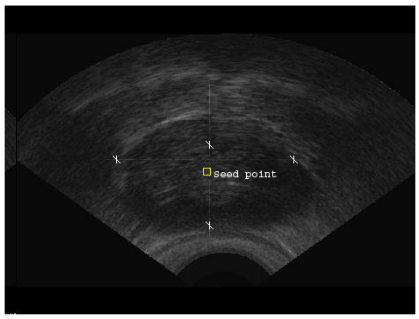

(b) Markers with the seed point

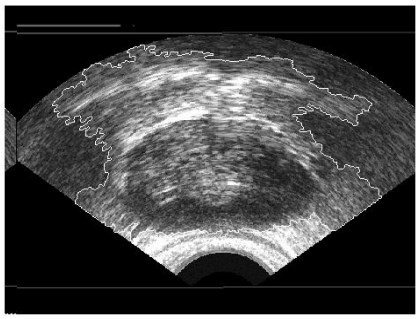

(c) Final segmented prostate

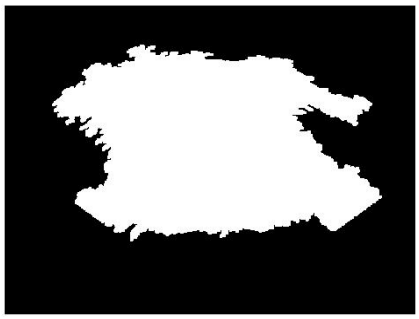

(d) Binary segmented

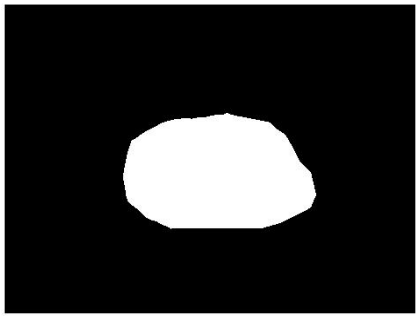

(e) Gold standard

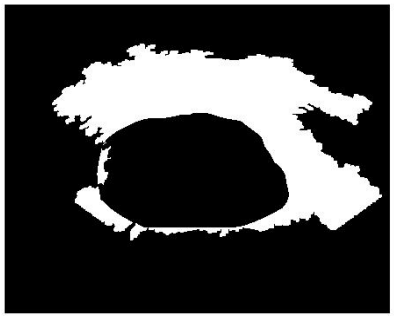

(f) Difference between gold standard and binary segmented prostate

Figure 5.4: Automated conventional region growing results for image 1

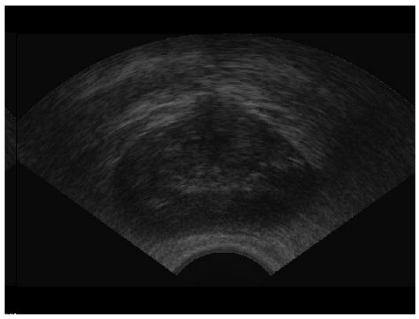

(a) Original image

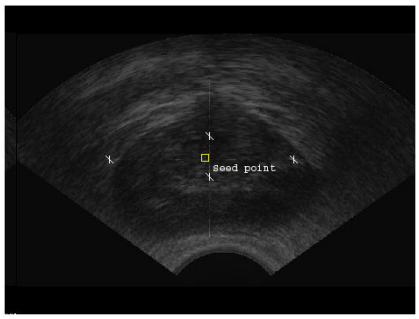

(b) Markers with the seed point

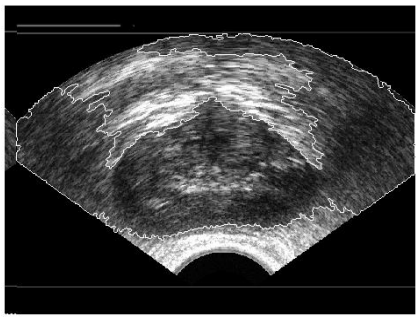

(c) Final segmented prostate

(d) Binary segmented

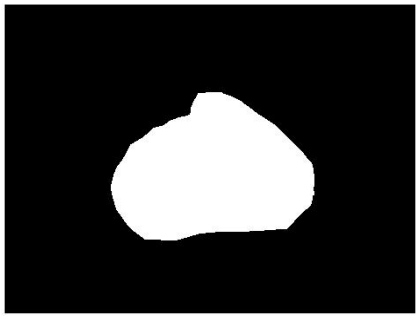

(e) Gold standard

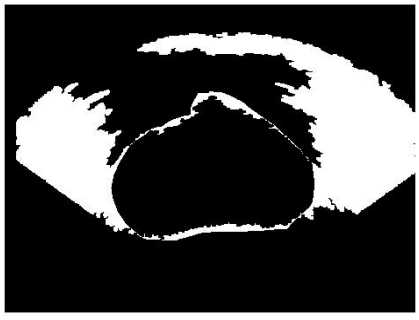

(f) Difference between gold standard and binary segmented prostate

Figure 5.5: Automated conventional region growing results image 2

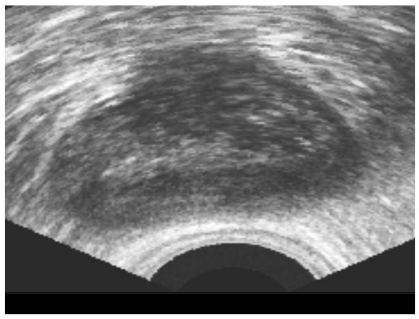

(a) Original image

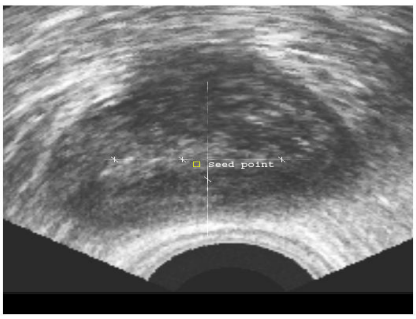

(b) Markers with the seed point

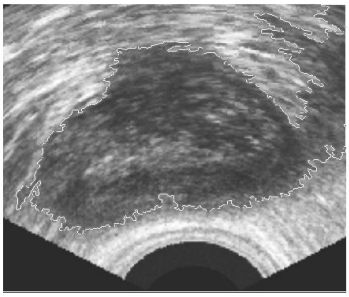

(c) Final segmented prostate

(d) Binary segmented prostate

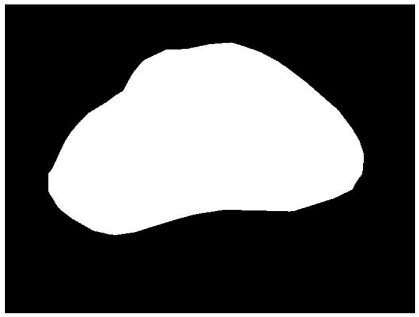

(e) Gold standard

(f) Difference between gold standard and the binary segmented prostate

Figure 5.6: Automated conventional region growing results for image 3

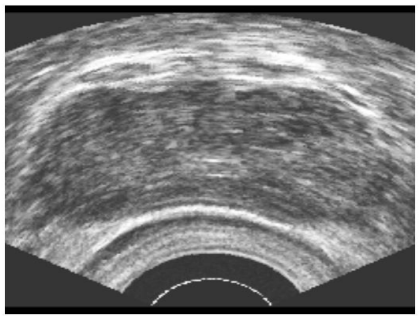

(a) Original image

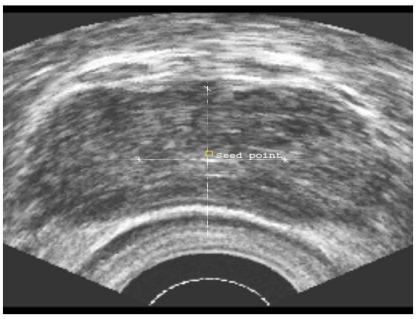

(b) Markers with the seed point

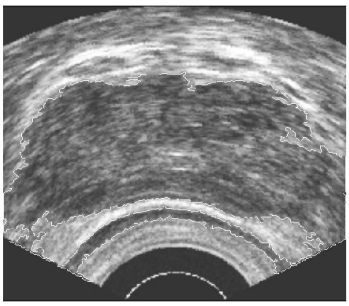

(c) Final segmented prostate

(d) Binary segmented prostate

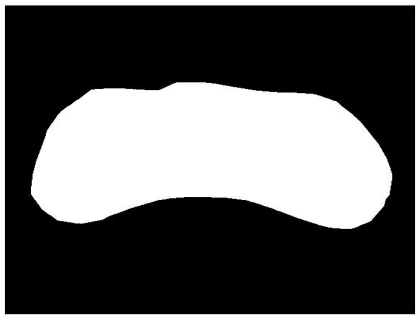

(e) Gold standard

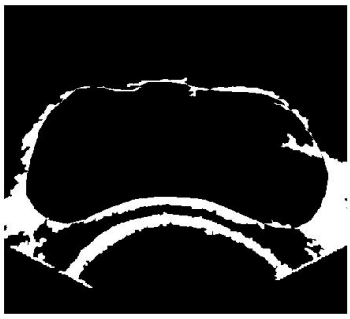

(f) Difference between gold standard and the binary segmented prostate

Figure 5.7: Automated conventional region growing results for image 4

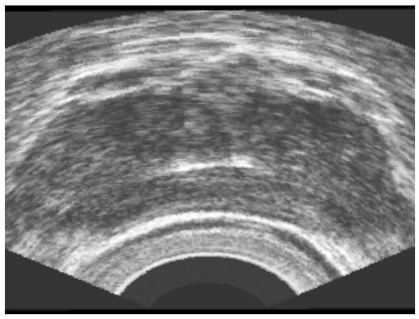

(a) Original image

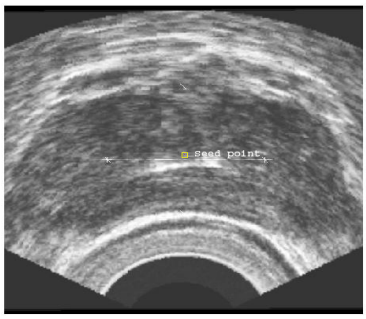

(b) Markers with the seed point

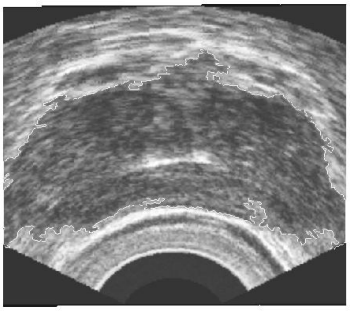

(c) Final segmented prostate

(d) Binary segmented prostate

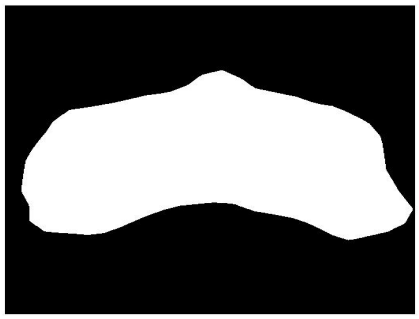

(e) Gold standard

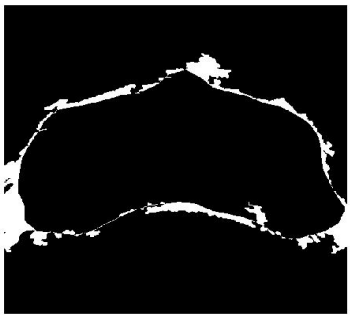

(f) Difference between gold standard and binary segmented prostate

Figure 5.8: Automated conventional region growing results for image 5

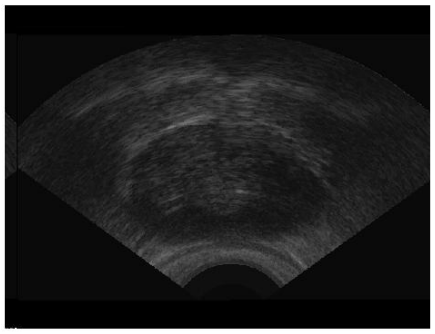

(a) Original image

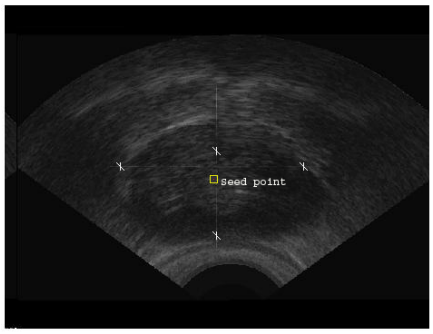

(b) Markers with the seed point

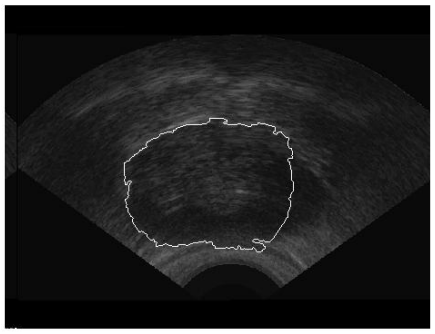

(c) Segmented prostate

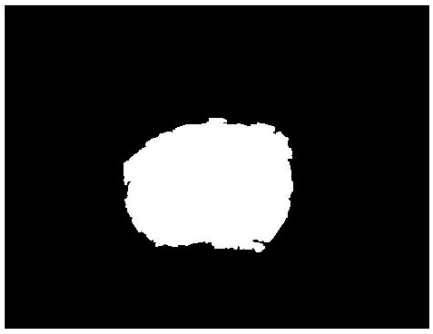

(d) Binary segmented prostate

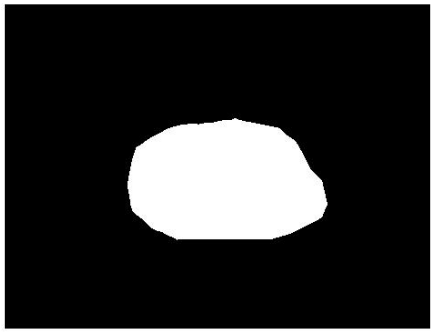

(e) Gold standard

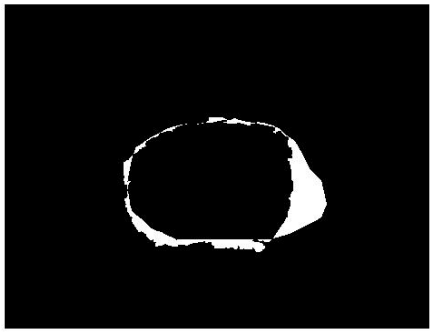

(f) Difference between gold standard and binary segmented

Figure 5.9: Automated modified region growing results for image 1

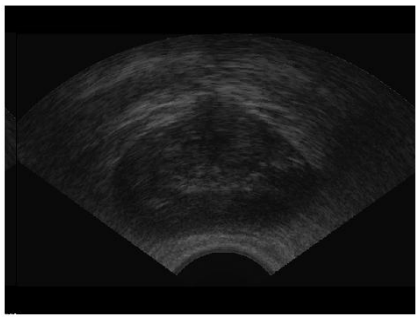

(a) Original image

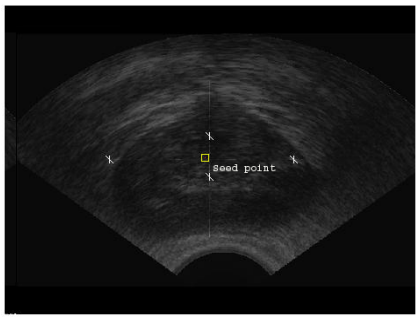

(b) Markers with the seed point

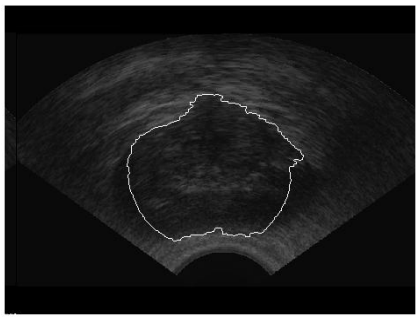

(c) Final segmented prostate

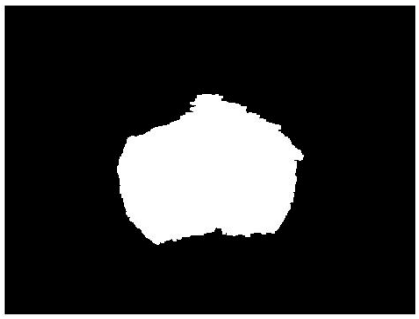

(d) Binary segmented prostate

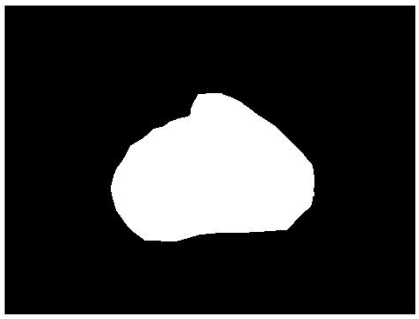

(e) Gold standard

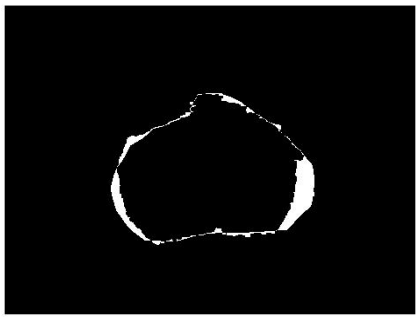

(f) Difference between gold standard and segmented binary

Figure 5.10: Automated modified region growing results for image 2

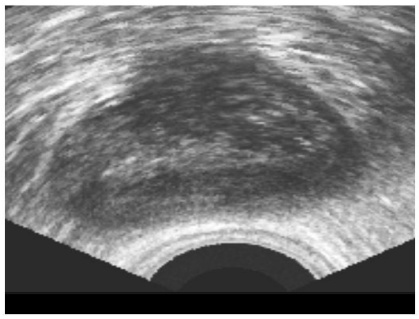

(a) Original image

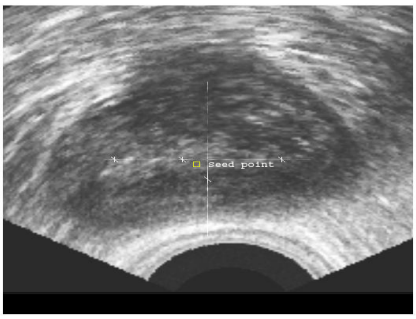

(b) Markers with the seed point

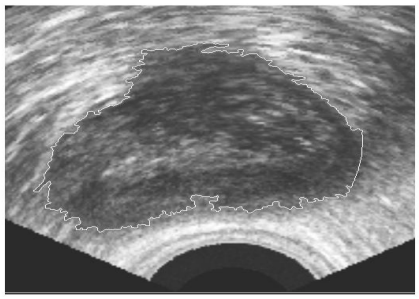

(c) Final segmented prostate

(d) Binary segmented prostate

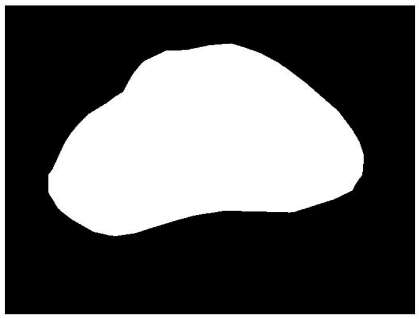

(e) Gold standard

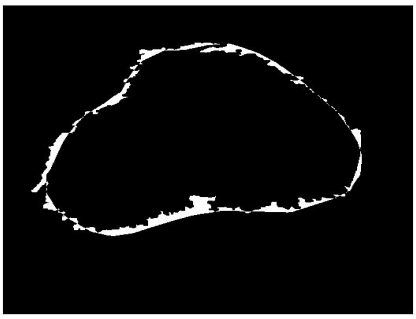

(f) Difference between gold standard and segmented binary

Figure 5.11: Automated modified region growing results for image 3

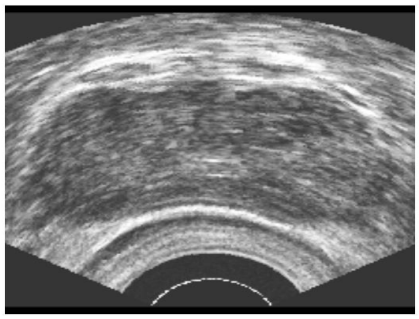

(a) Original image

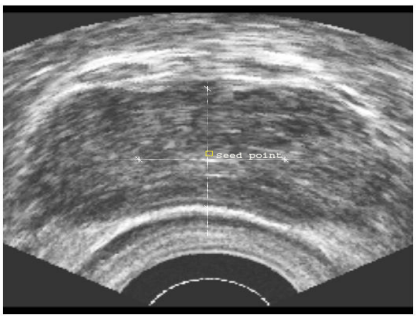

(b) Markers with the seed point

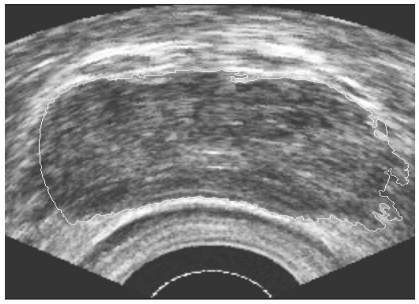

(c) Final segmented prostate

(d) Binary segmented prostate

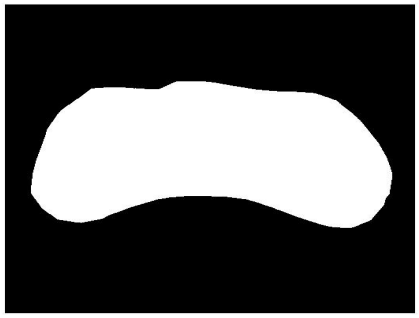

(e) Gold standard

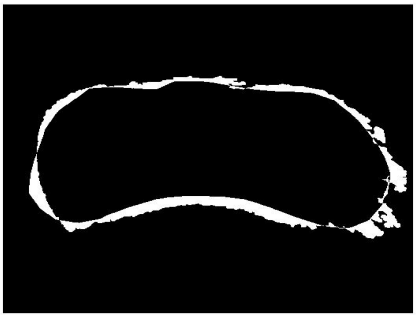

(f) Difference betweenthe gold standard and segmented binary

Figure 5.12: Automated modified region growing results for image 4

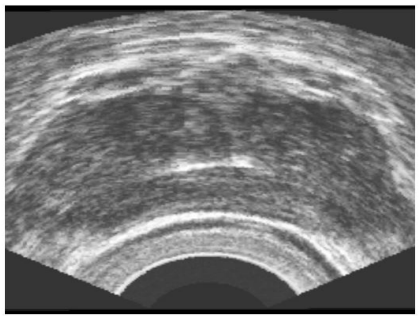

(a) Original image

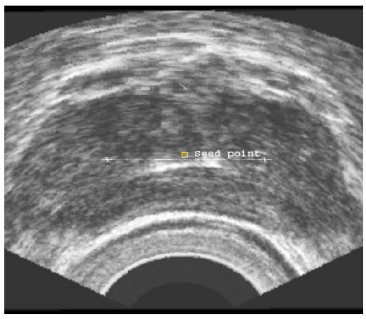

(b) Markers with the seed point

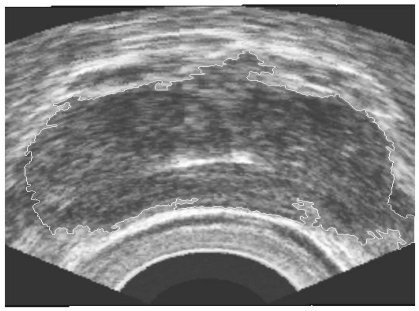

(c) Final segmented prostate

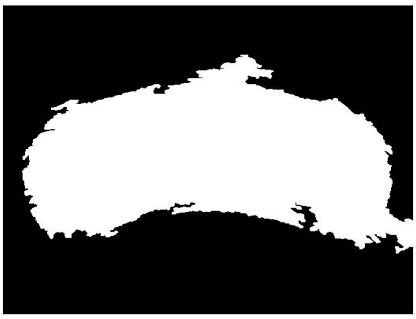

(d) Binary segmented prostate

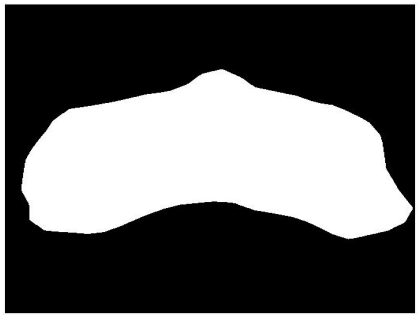

(e) Gold standard

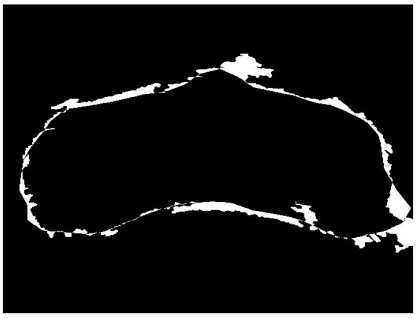

(f) Difference between the gold standard and segmented binary

Figure 5.13: Automated modified region growing results for image 5

Chapter 6

EXPERIMENTAL RESULTS

The automated proposed technique is implemented in Matlab, and it is applied to a set of thirty biomedical TRUS prostate images.

In this chapter, we compare between the automation of the region growing combined with the conventional region growing, the automated modified region growing, and the FCM technique, respectively. The results of applying the three techniques on different images are shown in Figs. 6.1-6.5.

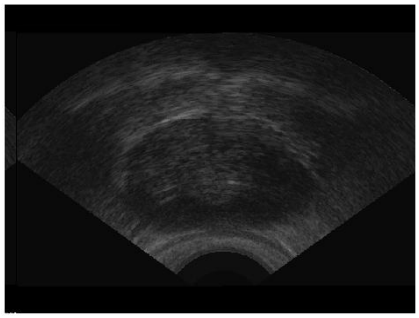

(a) Original image

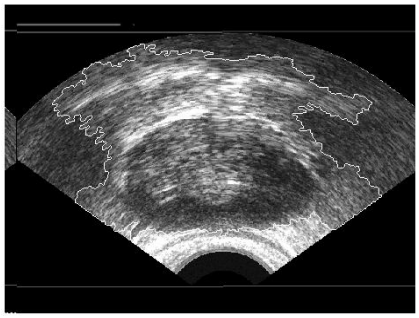

(b) Automated conventional region growing

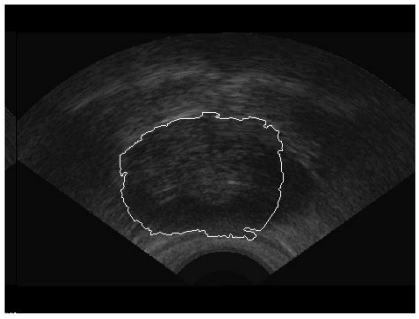

(c) Automated modified region growing

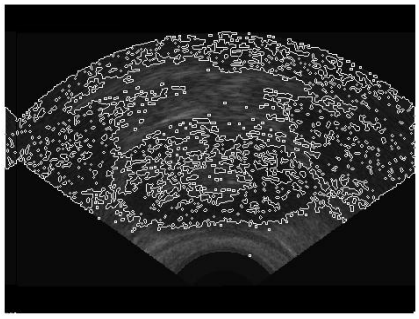

(d) FCM result

Figure 6.1: Image 1 results

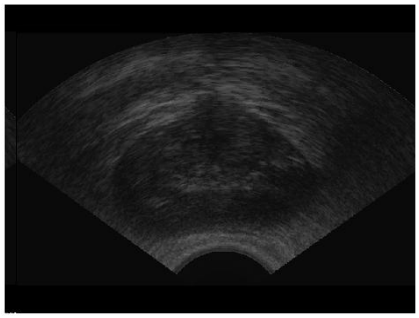

(a) Original image

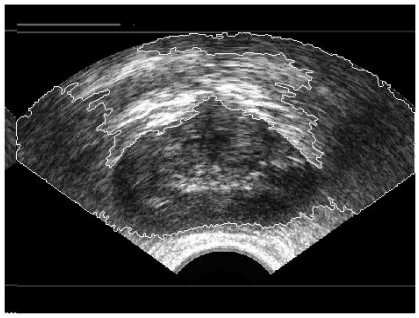

(b) Automated conventional region growing

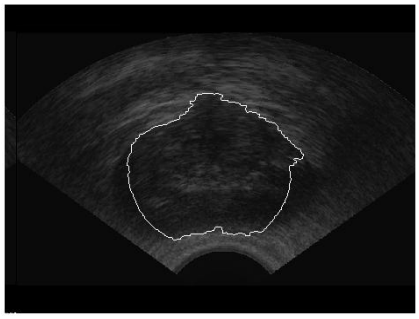

(c) Automated modified region growing

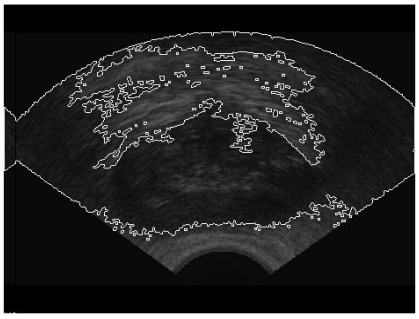

(d) FCM result

Figure 6.2: Image 2 results

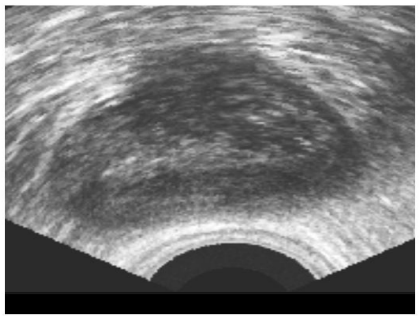

(a) Original image

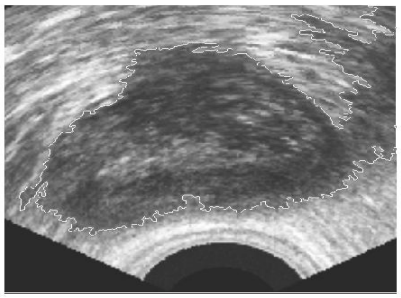

(b) Automated conventional region growing

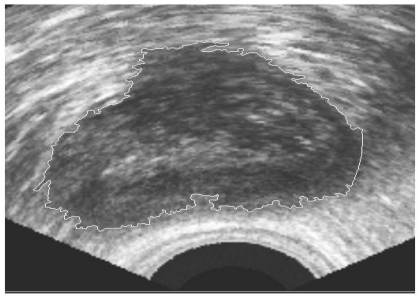

(c) Automated modified region growing

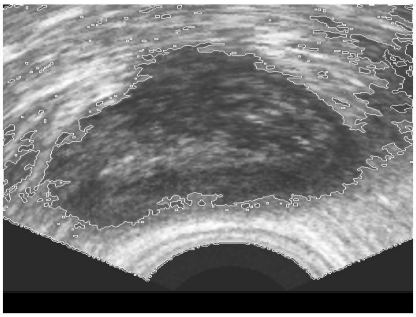

(d) FCM results

Figure 6.3: Image 3 results

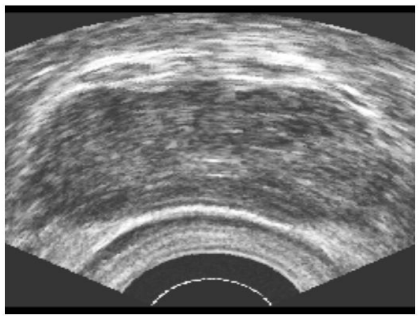

(a) Original image

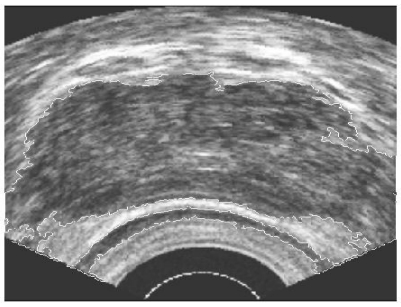

(b) Automated conventional region growing

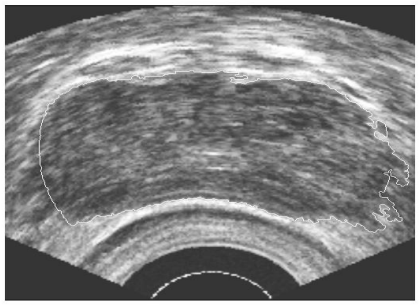

(c) Automated modified region growing

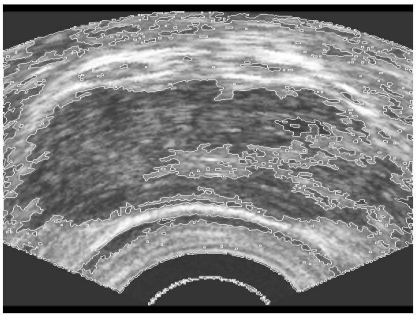

(d) FCM results

Figure 6.4: Image 4 results

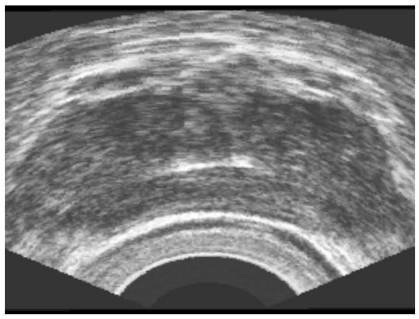

(a) Original image

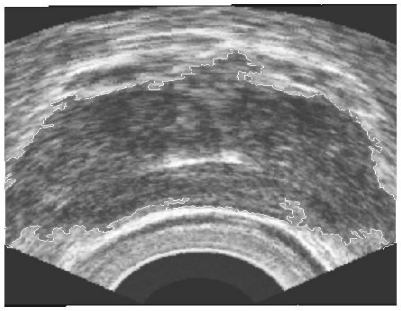

(b) Automated conventional region growing

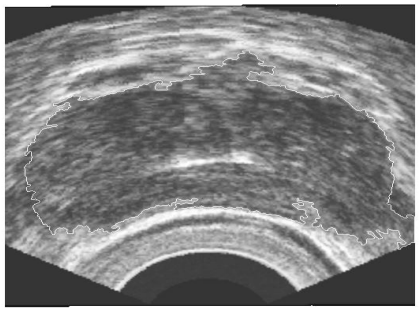

(c) Automated modified region growing

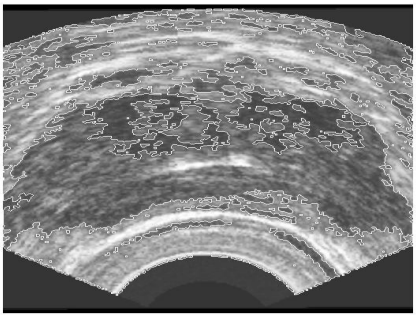

(d) FCM result

Figure 6.5: Image 5 results

6.1 Accuracy Measurement

In order to determine the quality of any technique, its accuracy should be measured. For segmentation, the accuracy is defined as the degree of closeness of the obtained segmentation results to its reference standard. The reference standard, in the case of medical images, is the radiology marking which is known as the gold standard.

There are different methods used for determining the accuracy of any medical image segmentation technique [44]. In this thesis, we calculated the accuracy by measuring the similarity between the obtained results and the gold standard according to eq. 6.1

$$accuracy = 1 - (\sum_{i=1}^{M}\sum_{j=1}^{N} B(i,j) \oplus G(i,j))/(M \times N) \tag{6.1}$$

where

G: The gold standard.

B: The binary segmented prostate.

$M \times N$: The size of G, which is the same as the size of B.

In this thesis, we used eq. 6.1 for calculating accuracy.

The accuracy results obtained by applying eq. 6.1 on the results of the three implemented techniques; FCM (chapter 4), automated conventional region growing (chapter 5), and automated modified region growing (chapter 5), are shown in Table 6.1.

Table 6.1 shows that the proposed automated modified region growing

technique introduces the highest accuracies in all images. For example, in image 1, it gives an accuracy of 97%, which is higher than FCM and the automated conventional region growing by 25% and 24%, respectively. Additionally, by observing the results in the table, it can be seen that both FCM and the automated conventional region growing give lower accuracies in case of very noisy images such as image 1 and image 2, while the proposed technique is not affected at all, and it gives the highest accuracies. This proves the superiority of the proposed technique. Also, it can be seen that the automated conventional region growing outperforms the FCM technique.

Table 6.1: Accuracy comparison between FCM, the automated conventional, and the automated modified region growing techniques.

Image number	FCM accuracy	Automated conventional region growing accuracy	Automated modified region growing accuracy
Image 1	72%	73%	97%
Image 2	74%	77%	98%
Image 3	89%	90%	97%
Image 4	82%	89%	95%
Image 5	80%	94%	95%

6.2 Time Measurement

Another factor for measuring the quality of the proposed technique is to compute the implementation time for both the FCM technique, and the automated modified region growing technique. Table 6.2 shows the implementation time for both techniques.

From Table 6.2, it is clearly seen that there is a significant difference in the time required for implementing both techniques. The time required for implementing the proposed automated modified region growing technique is greatly less than that required for FCM implementation. For example, in image 1, the time required for the proposed technique is only 37.4 seconds, while the time required for FCM is about 26 minutes. It means that the proposed automated modified region growing technique saves time by an amount of 97.6%.

Table 6.2: Time comparison between FCM and the automated modified region growing techniques

Image number	FCM implementation time (sec)	Automated modified region growing implementation time (sec)
Image 1	1576.3	37.4600
Image 2	1554.8	55.0070
Image 3	3879.3	601.2120
Image 4	3794.2	887.3850
Image 5	3542.2	808.2990

Chapter 7

CONCLUSION AND FUTURE WORK

7.1 Conclusion

Prostate ultrasound images are widely used in many clinical applications, hence, accurate delination of the prostate is a critical issue for these medical applications such as the prostate biopsy. There are many limitations that can affect the segmentation of ultrasound images such as low contrast, speckle noise, and fuzzy boundaries. Therefore, an automatic, accurate, fast, and robust segmentation technique is strongly needed. In this thesis, we have proposed a new technique for the prostate segmentation. The proposed technique is mainly based on the region growing technique, which is widely used in medical image segmentation. However, the proposed technique is

considered a modification for the conventional region growing technique in two main issues. First, the proposed technique overcomes the manual interaction problem associated with the region growing technique by selecting the seed point automatically. The interesting concept of this thesis is that it has a different segmentation perspective because it does not consider the speckle as noise needs to be removed before performing segmentation. Instead, the proposed technique considers the speckle as a signal carrying intensity information. It makes use of this information in determining the markers used for automatically selecting the seed point. Second, the stopping criteria relies on two parameters, and not only one like the conventional region growing technique. These parameters are the intensity, and the new parameter is the spatial Euclidean distance. Involving the spatial Euclidean distance makes the proposed technique more accurate and robust to the noise in ultrasound images. By conducting extensive performance evaluation, the proposed technique proves to give higher accuracies than those obtained by the automated conventional region growing or the FCM technique. In this thesis, an average similarity of 96.4% with gold standards was achieved, which is very high for these type of images (ultrasound images).

Moreover, the proposed technique saves time compared to the manual segmentation, which takes up to 20 minutes to be performed. Also, when compared to the time required for implementing FCM , it is found to be a time- saving technique.

Those advantages make the proposed technique a good candidate for daily

clinical purposes as it is automated, fast, robust, and accurate.

7.2 Future Work

Our future work will include integrating the proposed automated modified region growing technique with other segmentation techniques that suffer from the initialization problem such as deformable model technique to eliminate the need of manual interaction.

The proposed technique can also be efficiently applied to the segmentation of breast ultrasound images to help in detecting tumors in case of breast cancer, which becomes a common disease in the last few decades.

The proposed technique is applied to 2D TRUS images and can be extended to 3D TRUS images, where it may help in obtaining new valuable information from the images.

Bibliography

[1] Y. J. Zhang, "An overview of image and video segmentation in the last 40 years," *Proceedings of the 6th International Symposium on Signal Processing and Its Applications*, pp. 148-151, 2001.

[2] J. Alison Noble, and Djamal Boukerroui, "Ultrasound Image Segmentation: A Survey," *IEEE Transactions On Medical Imaging*, vol. 25, no. 8, August 2006.

[3] http://en.wikipedia.org/wiki/Ultrasound_imaging.

[4] T. L. Szabo, "Diagnostic Ultrasound imaging: Inside out," *Elseveir*, 2004.

[5] J. A. Jensen, "Medical ultrasound imaging," *Journal of Progress in Biophysics and Molecular Biology*, vol. 93, pp. 153-165, August 2006.

[6] T. Eltoft, "Speckle: modeling and filtering," *in Norwegian Signal Processing Symposium*, Norway, October 2003. [Online] Available: http://www.norsig.no/norsig2003/.

[7] A. Achim, A. Bezerianos, and P. Tsakalides, "Novel Bayesian multiscale method for speckle removal in medical ultrasound images," *IEEE Transaction on Medical Imaging*, vol. 20, no. 8, pp. 772–783, August 2001.

[8] S. Gupta, R. C. Chauhan, and S. C. Sexana, "Wavelet-based statistical approach for speckle reduction in medical ultrasound images," *Journal of Medical and Biological Engineering and Computing*, vol. 42, pp. 189–192, 2004.

[9] C.-Y. Xiao, S. Zhang, and Y.-Z. Chen, "A diffusion stick method for speckle suppression in ultrasonic images," *Pattern Recognition Letter*, vol. 25, no. 16, pp. 1867–1877, December 2004.

[10] K. Z. Abd-Elmoniem, A.-B. M. Youssef, and Y. M. Kadah, "Realtime speckle reduction and coherence enhancement in ultrasound imaging via nonlinear anisotropic diffusion," *IEEE Transaction on Biomedical Engineering*, vol. 49, no. 9, pp. 997–1014, September 2002.

[11] M. Karaman, M. Alper Kutay, and G. Bozdagi, "An adaptive speckle suppression filter for medical ultrasonic imaging," *IEEE Transactions on Medical Imaging*, vol. 14, pp. 283–292, June 1995.

[12] C. Tauber, H. Batatia, and A. Ayache, "A robust speckle reducing anisotropic diffusion," *IEEE International Conference on Image Processing*, Singapore, vol. 1, pp. 247–250, 2004.

[13] http://www.cancer.gov/Templates/db_alpha.aspx?CdrID=46632.

[14] http://www.mayoclinic.com/health/ultrasound/PR00053.

[15] D. L. Pham, C. Xu, and J. L. Prince, "A survey of current methods in medical image segmentation," *Annual Review of Biomedical Engineering*, 1998.

[16] D. J. Withey, and Z.J. Koles, "Medical image segmentation: Methods and software," *Joint Meeting of the 6th International Symposium on Noninvasive Functional Source Imaging of the Brain and Heart and the International Conference on Functional Biomedical Imaging*, pp. 140-143, 2007.

[17] S. Lakare, and A. Kaufman, "3D segmentation techniques for medical volumes," *Center for Visual Computing, Department of Computer Science, State University of New York*, Dec. 2000.

[18] R. Gonzalez, and R. Woods, "Digital image processing," *Prentice Hall*, 2001.

[19] http://www.vuse.vanderbilt.edu/~mip-web/seminar_files/GraphCuts.

[20] G. Hamarneh, "Towards intelligent deformable models for medical image analysis," Ph.D. Thesis*, Department of Signals and Systems, School of Electrical and Computer Engineering, Chalmers University of Technology*, 2001.

[21] D. Terzopoulos and D. Metaxas, "Dynamic 3D models with local and global deformations: Deformable superquadrics," *IEEE Transactions on*

Pattern Analysis and Machine Intelligence, vol. 13, no. 7, pp. 703-714, July 1991.

[22] E. A. T. O'Donnell, "Extruded generalized cylinder: A deformable model for object recovery," *In Proceeding of Computer Vision and Pattern Recognition* Conference, pp. 174 - 181, 1994.

[23] I. Cohen, L. D. Cohen, and N. Ayache, "Using deformable surfaces to segment 3D images and infer differential structures," *Computer Vision, Graphics, and Image Processing: Image Understanding*, vol. 56, no. 2, pp. 242-263, September 1992.

[24] T. McInerney and D. Terzopoulos, "A dynamic finite element surface model for segmentation and tracking in multidimensional medical images with application to cardiac 4D image analysis," *Journal of Computerized Medical Imaging and Graphics*, vol. 19, no. 1, pp. 69-83, 1995.

[25] T. McInerney and D. Terzopoulos, "Deformable models in medical image analysis: A survey," *Medical Image Analysis*, pp.91-108, 1996.

[26] D. L. Pham, C. Xu, and J. L. Prince, "Image segmentation using deformable models," *Handbook of Medical Imaging, Chapter 3*, 2000.

[27] http://math.berkeley.edu/~sethian/2006/Explanations/level_set_explain.html.

[28] O. Wirjadi, "Survey of 3D image segmentation methods," *Models and Algorithms in Image Processing Fraunhofer ITWM*, no. 123, 2007.

[29] V. Caselles, R. Kimmel, and G. Sapiro, "Geodesic Active Contours," *International Journal of Computer Vision*, vol. 22, no. 1, pp. 61-79, 1995.

[30] http://campar.in.tum.de/twiki/pub/Chair/TeachingSs04SeminarImaging/11Segmentation.pdf.

[31] http://ranger.uta.edu/~hchen/CSE6366/students'%20presentations/Jean/dippresentation.ppt.

[32] H. D. Cheng, X. Cai, X. Chen, L. Hu, and X. Lou, "Computer-aided detection and classification of microcalcifications in mammograms: A survey," *Pattern Recognition Society journal*, vol. 36, no. 12, pp. 2967-2991, December 2003.

[33] R. Xu, and D.Wunsch, "Survey of clustering algorithms," *IEEE Transactions on Neural Networks*, vol. 16, no. 3, May 2005.

[34] Y. Feng, and W. Chun, "Brain MR image segmentation using fuzzy clustering with spatial constraints based on Markov random field theory," *Lecture Notes In Computer Science LNCS*, vol. 3150, pp. 188-195, 2004.

[35] http://www.slicer.org.

[36] K. Pohl, S. Bouix, M. Shenton, W. Grimson, and R. Kikinis, "Automatic segmentation using non-rigid registeration," *In the Proceedings of the 8th International Conference on Medical Image Computing and Computer Assisted Intervention*, 2005.

[37] F. Karray, and C. Silva, "Soft computing and intelligent system design," *Addison Wesley*, 2004.

[38] http://www.disi.unige.it/person/ChiarabiniL/presentazione.ppt.

[39] http://homepages.inf.ed.ac.uk/rbf/CVonline/LOCAL_COPIES/KIM1/Seminars/Watershed/sld001.htm.

[40] A. R. Abdel-Dayem, and M. R. El-Sakka, "Fuzzy c-means clustering for segmenting carotid artery ultrasound images," *In the proceedings of the 4th International Conference on Image Analysis and Recognition,* ICIAR2007, pp. 935-948, 2007.

[41] H. Liu, C. Xie, Z. Chen, and Y. Lei, "Segmentation of ultrasound image based on morphological operation and fuzzy clustering," *Proceedings of the 3rd IEEE International Workshop on Electronic Design, Test and Applications*, 2006.

[42] A. I. SHIHAB, "Fuzzy clustering algorithms and their application to medical image analysis," *Ph.D. Thesis, University of London*, December 2000.

[43] E. Cuevas, D. Zaldivar, and R. Rojas, "Fuzzy segmentation applied to face segmentation," available at http://page.mi.fu-berlin.de/zaldivar/files/tr-b-04-09.pdf, 2004.

[44] http://en.wikipedia.org/wiki/Accuracy.